This study aimed to clarify the impact of diastolic regurgitation from PA to RV on ventricular energetics by conducting a theoretical analysis using computational models.

Methods

We modeled the cardiovascular systems of the Norwood procedure using the SPS, and valved and non-valved RV-PA shunts. The electrical analogs of the models used to simulate the cardiovascular systems are shown in Fig. 1. We modeled the postoperative cardiovascular systems mathematically by a combination of the time-varying elastance cardiac chamber model and the three-element Windkessel vascular model.

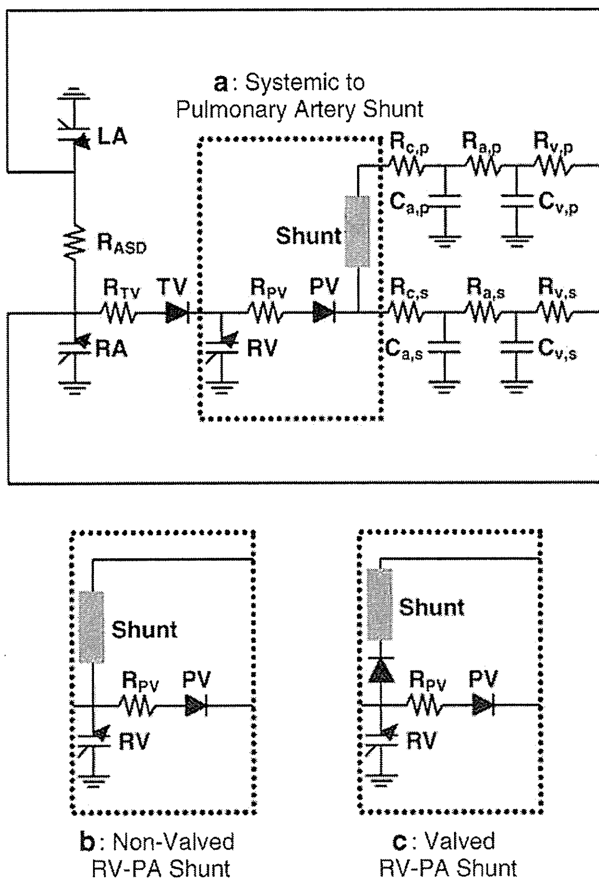

Fig. 1 Electrical analogs of Norwood procedures. **a** Norwood procedure with systemic to pulmonary shunt, **b** Norwood procedure with non-valved right ventricle to pulmonary artery (RV-PA) shunt, **c** Norwood procedure with valved RV-PA shunt. *LA* left atrium, *RA* right atrium, *RV* right ventricle, *PV* pulmonary valve, *TV* tricuspid valve, *ASD* atrial septal defect. R_a arterial resistance, R_c characteristic impedance, R_v venous resistance, C_a arterial capacitance, C_v venous capacitance. *s* and *p* systemic and pulmonary circulation, respectively. R_{PV}, R_{TV} and R_{ASD} resistance at PV, TV and ASD, respectively

Heart

The right ventricular and atrial chambers are represented by the time-varying elastance model [5–7]. The end-systolic pressure–volume relationship is described by a linear equation:

$$P_{es,cc} = E_{es,cc}[V_{es,cc} - V_{0,cc}] \tag{1}$$

where $P_{es,cc}$ is end-systolic pressure, $V_{es,cc}$ is end-systolic volume, $E_{es,cc}$ is the maximal volume elastance, $V_{0,cc}$ is the volume at which end-systolic pressure is equal to 0 mmHg, and cc denotes the right atrial (RA), left atrial (LA), or right ventricular (RV) chamber. The end-diastolic pressure–volume relationship is represented by a non-linear equation:

$$P_{ed,cc} = A_{cc}[e^{B_{cc}(V_{ed,cc} - V_{0,cc})} - 1] \tag{2}$$

where $P_{ed,cc}$ is end-diastolic pressure, $V_{ed,cc}$ is end-diastolic volume, A_{cc} and B_{cc} are constants [5–7]. We assumed the time course of elastance by defining normalized elastance curve $e_{cc}(t)$ as follows:

$$\begin{aligned} e_{cc}(t) &= 0.5\,[1 - \cos(\pi t/T_{es,cc})] \quad (0 \le t < 2T_{es,cc}) \\ e_{cc}(t) &= 0 \quad (2T_{es,cc} \le t < T_c) \end{aligned} \tag{3}$$

where t is the time from the start of systole, $T_{es,cc}$ is the time to the end of systole, and T_c is the duration of cardiac cycle. Using $e_{cc}(t)$, the instantaneous pressure–volume relationship is described by:

$$P_{cc}(t) = [P_{es,cc}(V_{cc}) - P_{ed,cc}(V_{cc})]e_{cc}(t) + P_{ed,cc}(V_{cc}) \tag{4}$$

Ventricular systole is preceded by atrial systole. The time advance of atrial systole (DT) is calculated as a fixed fraction of T_c (DT = 0.02 T_c) [9]. The function of each chamber is characterized by the parameters $E_{es,cc}$, $T_{es,cc}$, $V_{0,cc}$, A_{cc}, B_{cc} and $e_{cc}(t)$. The same $e_{cc}(t)$ is used for all chambers, but the other parameters are different between chambers, as shown in Table 1. Nonrestrictive atrial septal defect is described as constant resistance (R_{ASD}). Each valve is represented as an ideal diode connected serially to a small resistor (pulmonary R_{PV}, tricuspid R_{TV}).

Vascular system

Basically, the pulmonary and systemic circulations are modeled as modified Windkessel impedances. Each vascular system is modeled by lumped venous (C_v) and arterial (C_a) capacitances, a characteristic impedance (R_c) that is related to the stiffness of the proximal aorta or pulmonary artery, a lumped arterial resistance (R_a), and a

Table 1 Parameters used in modeling

Heart rate (HR) (beats/min)	160		
Duration of cardiac cycle (T_c) (ms)	375		
Time to end systole (T_{es}) (ms)	RV: 136	RA: 56	LA: 56
End-systolic elastance (E_{es}) (mmHg/ml)	RV: 8.5	RA: 7.35	LA: 7.35
Scaling factor of EDPVR (A) (mmHg)	RV: 0.9	RA: 0.17	LA: 0.17
Exponent for EDPVR (B) (ml^{-1})	RV: 0.062	RA: 0.484	LA: 0.484
Unstressed volume (V_0) (ml)	RV: 4	RA: 1	LA: 1
Valvular resistance (forward) (mmHg s ml^{-1})	Pulmonary: 0.0004	Tricupsid: 0.00004	
Resistance (mmHg s ml^{-1})	ASD: 0.001		
Index of pure viscous effects (k_1) [mmHg $(l/s)^{-1}$ mm^4]	Shunt: 5.76×10^4		
Index of convective acceleration (k_2) [mmHg $(l/s)^{-2}$ mm^4]	Shunt: 1.87×10^7		
Arterial resistance (R_a) (mmHg s ml^{-1})	Systemic (s): 3.83	Pulmonary (p): 0.63	
Characteristic impedance (R_c) (mmHg s ml^{-1})	Systemic (s): 0.20	Pulmonary (p): 0.028	
Venous resistance (R_v) (mmHg s ml^{-1})	Systemic (s): 0.083	Pulmonary (p): 0.011	
Arterial capacitance (C_a) (ml/mmHg)	Systemic (s): 0.50	Pulmonary (p): 0.31	
Venous capacitance (C_v) (ml/mmHg)	Systemic (s): 4.39	Pulmonary (p): 0.89	

RV right ventricle, *RA* right atrium, *LA* left atrium, *EDPVR* end-diastolic pressure–volume relation, *ASD* atrial septal defect

resistance proximal to C_v (R_v). This framework is similar to that used in deriving Guyton's resistance to venous return [8]. Arterial and venous capacitors for systemic circulation are denoted by $C_{a,s}$ and $C_{v,s}$, respectively, and those for pulmonary circulation by $C_{a,p}$ and $C_{v,p}$. The ratio of C_a to C_v is obtained from previous reports [6, 9, 10].

The relation between pressure (P_c) and volume (V_c) in each capacitance is described by the following linear equation:

$$P_c = \frac{V_c}{C} \quad (5)$$

The change in volume in each capacitance [$\mathrm{d}V(t)/\mathrm{d}t$] is described by the differential equation below:

$$\frac{\mathrm{d}V(t)}{\mathrm{d}t} = \sum Q_{\mathrm{inflow}}(t) - \sum Q_{\mathrm{outflow}}(t) \quad (6)$$

where $Q_{\mathrm{inflow}}(t)$ and $Q_{\mathrm{outflow}}(t)$ indicate the instantaneous volumetric flow rates at the inlet and outlet, respectively, of each compartment.

Pressure drop across the shunt

Flow of non-Newtonian fluid in a curved pipe is approximated as a quadratic function of $Q(t)$ [11, 12]. The instantaneous pressure drop across the shunt is described by:

$$\Delta P(t) = \frac{k_1 Q(t) + k_2 Q^2(t)}{D^4} \quad (7)$$

where $\Delta P(t)$ (mmHg) is pressure drop across the shunt, $Q(t)$ (l/s) is the instantaneous volume flow rate in shunt, D (mm) is the shunt diameter, k_1 [mmHg $(l/s)^{-1}$ mm^4] is the index of pure viscous effects and k_2 [mmHg $(l/s)^{-2}$ mm^4] is the index of convective acceleration [9].

Protocols

First, the control state was simulated using the 4.0-mm SPS model. Total stressed blood volume (V_s), which is the sum of the stressed volumes in all capacitances and in all chambers, was set as 80 ml.

$$V_s = V_{RV} + V_{LA} + V_{RA} + V_{C_{a,s}} + V_{C_{v,s}} + V_{C_{a,p}} + V_{C_{v,p}} \quad (8)$$

We solved the simultaneous differential equations (Eqs. 1–8) using MATLAB (MathWorks).

Shunt diameter (D) was decreased stepwise from 4.0 to 3.0 mm at decrements of 0.5 mm in the SPS model and increased from 4.0 to 6.0 mm at increments of 1.0 mm in both the valved and non-valved RV-PA shunt models. RV forward flow, systemic and pulmonary flows (Q_s and Q_p), systemic and pulmonary arterial pressures (SAP and PAP), right ventricular end-diastolic volume (RVEDV), stroke work (SW), systolic pressure–volume area (PVA) and mechanical efficiency after each procedure were calculated for each shunt diameter. Heart rate and mean SAP were set at the same values as those of the control state, by adjusting the total stressed blood volume (V_s).

Calculation of arterial and venous oxygen saturation

Since the total amount of O_2 present in the atrium is preserved and the decrease in O_2 content in blood balances the whole body O_2 consumption, arterial (SaO_2) and venous O_2 saturation (SvO_2) are calculated by the following equations for Q_p and Q_s (l/min):

$$SaO_2 = S_{PV}O_2 - \frac{CVO_2 \times BSA}{1.34 \times Hb \times 10 \times Q_p}$$

$$SvO_2 = SaO_2 - \frac{CVO_2 \times BSA}{1.34 \times Hb \times 10 \times Q_s}$$

where $S_{PV}O_2$ is the pulmonary venous O_2 saturation, CVO_2 (ml O_2/min/m^2) is the whole body O_2 consumption, BSA (m^2) is the body surface area, and Hb (g/dl) is the hemoglobin concentration. The constant 10 (dl/l) converts l to dl, and 1.34 (ml O_2/g) converts hemoglobin content to oxygen content. The following assumptions are used in the O_2 calculation: $S_{PV}O_2 = 0.97$ (dimensionless), $CVO_2 = 185$ ml O_2/min/m^2, BSA $= 0.20$ m^2 and Hb $= 16.0$ g/dl [9, 13].

Results

The hemodynamic parameters obtained from the computational simulations are shown in Table 2.

Although the increase in shunt diameter caused an increase in systolic SAP and a decrease in diastolic SAP in the SPS model, changes in shunt diameter only affect systolic and diastolic SAP slightly in both the valved and non-valved RV-PA shunt models. Despite the use of small caliber shunt in the SPS model, mean PAP, Q_p and Q_p/Q_s were higher than in both valved and non-valved RV-PA shunt models. Mean PAP, Q_p and Q_p/Q_s in the 3.5-mm SPS model were higher than those in the 6.0-mm non-valved RV-PA shunt model and almost equivalent to those in the 5.0-mm valved RV-PA shunt model.

Right ventricular pressure, SAP, PAP, aortic flow, and shunt flow in the 3.5-mm SPS, 6.0-mm non-valved shunt, and 5.0-mm valved RV-PA shunt models are shown in Fig. 2. In both valved and non-valved RV-PA shunt models, RV ejection to pulmonary circulation through the shunt preceded RV ejection to systemic circulation and continued even after the end of ejection to systemic circulation. Comparisons of the hemodynamics of the 3.5-mm SPS, and 5.0-mm valved and 6.0-mm non-valved RV-PA shunt models are shown in Fig. 3. RVEDV was smaller in the 6.0-mm non-valved RV-PA shunt (−3.7%) and the 5.0-mm valved RV-PA shunt (−11.7%) models than that in the 3.5-mm SPS model. At the same shunt diameter, mean PAP, Q_p, Q_p/Q_s, SaO_2 and SvO_2 were higher with the valved RV-PA shunt than with the non-valved shunt.

In the SPS model, the use of a larger conduit significantly increased systemic-to-pulmonary diastolic run-off and RVEDV (Table 2). In the valved and non-valved RV-PA shunt models, increase in conduit size likewise

Table 2 Hemodynamic data obtained from computational simulation of SPS, non-valved RV-PA shunt, and valved RV-PA shunt

	Mathematical models								
	SPS			Non-valved RV-PA			Valved RV-PA		
Shunt diameter (mm)	3.0	3.5	4.0	4.0	5.0	6.0	4.0	5.0	6.0
Heart rate (beats/min)	160			160			160		
Systolic systemic artery pressure (mmHg)	83.9	87.0	90.9	75.7	76.3	77.0	75.7	76.2	76.9
Diastolic systemic artery pressure (mmHg)	46.6	45.0	43.4	51.9	51.9	51.9	51.9	51.8	51.9
Mean systemic artery pressure (mmHg)	58.6	58.7	58.7	58.7	58.7	58.7	58.7	58.7	58.7
Mean PA pressure (mmHg)	10.4	13.8	17.3	7.50	9.83	11.9	8.98	12.6	16.2
RV forward flow (l/min)	1.60	1.86	2.14	1.53	1.86	2.19	1.51	1.81	2.10
Q_p (l/min)	0.77	1.04	1.32	0.55	0.73	0.90	0.68	0.98	1.27
Q_s (l/min)	0.83	0.82	0.82	0.83	0.83	0.83	0.83	0.83	0.83
Q_p/Q_s	0.94	1.26	1.62	0.66	0.88	1.09	0.81	1.18	1.54
Diastolic run-off (l/min)	0.52	0.69	0.85						
Diastolic regurgitation (l/min)				0.15	0.29	0.47			
SaO_2 (%)	74.7	80.4	83.9	65.4	73.5	77.8	71.5	79.3	83.4
SvO_2 (%)	53.9	59.5	62.8	44.8	52.8	56.9	50.8	58.5	62.5
Stressed blood volume (ml)	70.6	75.1	80.0	64.9	67.9	71.4	65.7	69.2	73.2
RVEDV (ml)	21.6	23.3	25.0	19.4	20.8	22.4	19.3	20.6	22.0
Stroke work (mmHg ml)	759	905	1,062	600	713	829	596	704	815
Systolic PVA (mmHg ml)	1,008	1,157	1,315	765	851	949	762	843	934
Mechanical efficiency (%)	75.3	78.2	80.8	78.4	83.8	87.4	78.3	83.5	87.2

SPS systemic to pulmonary artery shunt, *RV-PA* right ventricle to pulmonary artery shunt, *RV* right ventricle, *PA* pulmonary artery, Q_p pulmonary blood flow, Q_s systemic blood flow, SaO_2 arterial oxygen saturation, SvO_2 venous oxygen saturation, *RVEDV* right ventricular end-diastolic volume, *PVA* systolic pressure–volume area

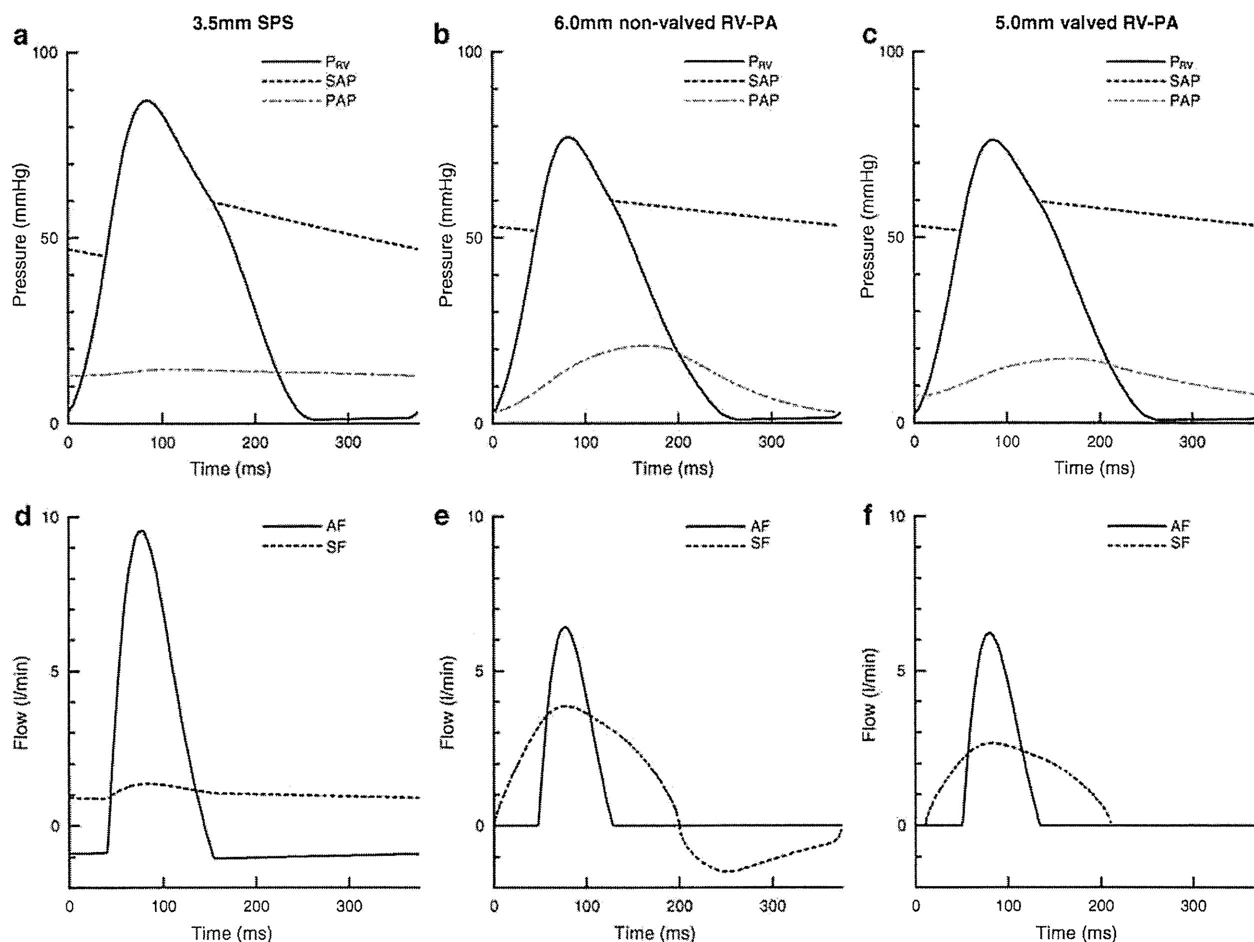

Fig. 2 Right ventricular pressure, systemic and pulmonary arterial pressures, aortic flow and shunt flow computed from the mathematical models of Norwood procedures with 3.5-mm systemic to pulmonary artery shunt (SPS **a**, **d**), 6.0-mm non-valved right ventricle to pulmonary artery (RV-PA) shunt (**b**, **e**), and 5.0-mm valved RV-PA shunt (**c**, **f**). P_{RV} right ventricular pressure, SAP systemic arterial pressure, PAP pulmonary arterial pressure, AF aortic flow, SF shunt flow

increased RVEDV, but the magnitudes were smaller than those of the SPS model, despite larger conduits being used in these models. The smaller RVEDV contributed to decreases in SW and PVA. The pressure–volume loops of the 3.5-mm SPS, and the 5.0-mm valved and 6.0-mm non-valved RV-PA shunt models are shown in Fig. 4. The SW in the 5.0-mm valved and 6.0-mm non-valved RV-PA shunts were −22.3 and −8.4%, respectively, smaller than that in the 3.5-mm SPS. The PVA in the 5.0-mm valved and 6.0-mm non-valved RV-PA shunts were −27.1 and −18.0%, respectively, smaller than that in the 3.5-mm SPS. Mechanical efficiency (SW/PVA) in the 5.0-mm valved and 6.0-mm non-valved RV-PA shunt were 5.3 and 9.2%, respectively, higher than that in the 3.5-mm SPS. Although the use of non-valved conduit caused diastolic regurgitation from PA to RV, there was no difference in mechanical efficiency between the valved and non-valved RV-PA shunts at the same shunt diameter. Furthermore, compared to the SPS and the valved RV-PA shunt, the non-valved RV-PA shunt delivered the highest mechanical efficiency at any given Q_p/Q_s (Fig. 5).

Discussion

The Norwood procedure for stage I palliation of the HLHS was first reported in 1983 [14]. In the conventional Norwood procedure, pulmonary circulation was maintained by a SPS, such as the modified Blalock–Taussig shunt. The development of the RV-PA shunt in the last decade has improved patient's mortality and morbidity [15]. Since Sano et al. [16] reported their experience with the non-valved RV-PA shunt in 2003, this modification has been widely used. However, it remains controversial whether the RV-PA shunt truly improves the outcome of the Norwood procedure.

The RV-PA shunt eliminates systemic to pulmonary diastolic run-off that occurs when using the SPS, which

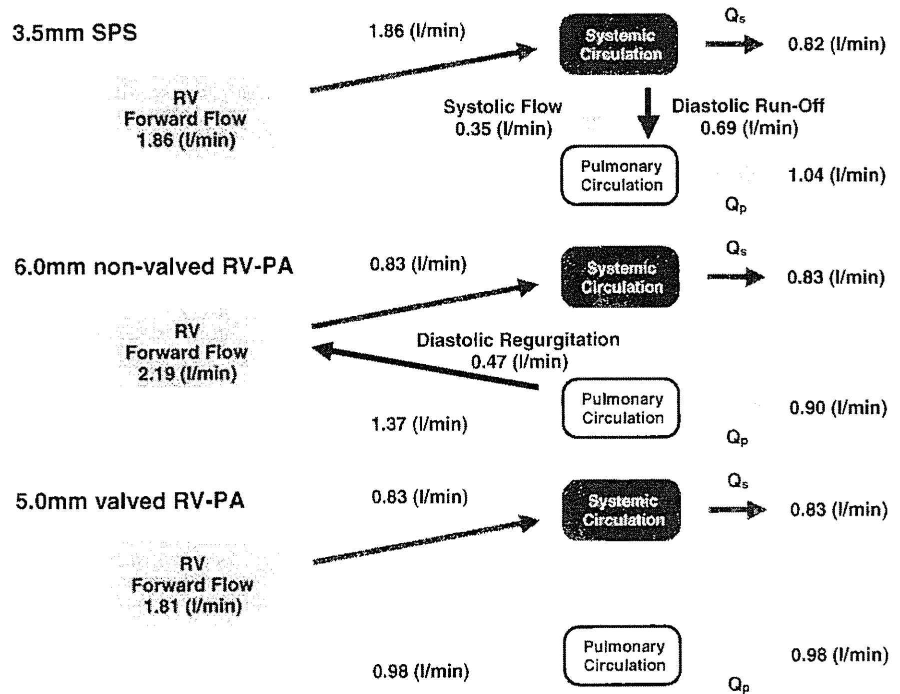

Fig. 3 Hemodynamics obtained from the 3.5-mm systemic-to-pulmonary shunt (*SPS*) model, and 6.0-mm non-valved and 5.0-mm valved right ventricle to pulmonary artery (*RV-PA*) shunt models

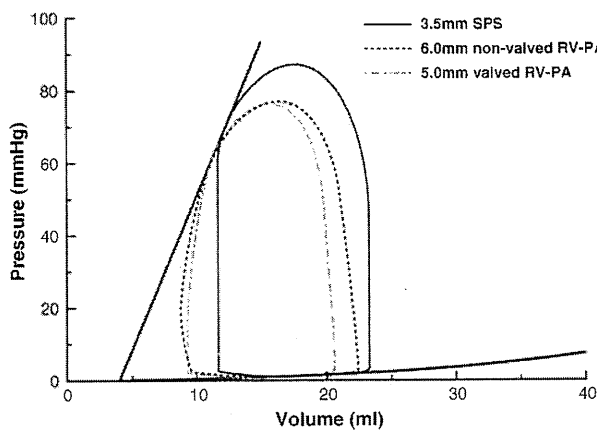

Fig. 4 Pressure-volume loops of simulated Norwood procedures. *Solid line* 3.5-mm systemic to pulmonary artery shunt (SPS), *dotted line* 6.0-mm non-valved right ventricle to pulmonary artery (RV-PA) shunt, *dot-dashed line* 5.0-mm valved RV-PA shunt

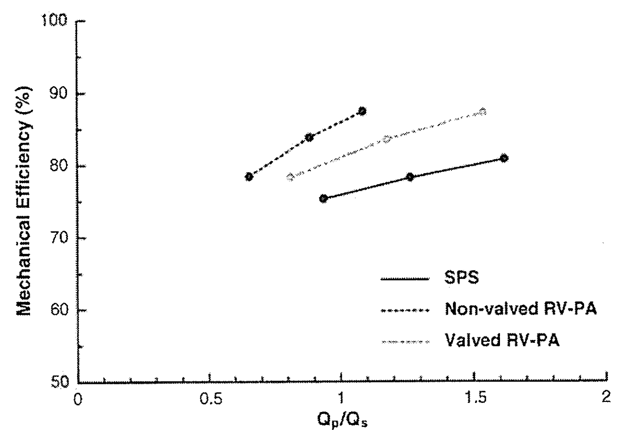

Fig. 5 The relation between Q_p/Q_s and mechanical efficiency. *Solid line* systemic to pulmonary artery shunt (SPS), *dotted line* non-valved right ventricle to pulmonary artery (RV-PA) shunt, *dot-dashed line* valved RV-PA shunt

causes a massive increase in ventricular preload. However, diastolic regurgitation from PA to RV is a drawback of the non-valved RV-PA shunt. Thus, some authors have reported the advantages of a valved RV-PA shunt [3, 4, 17]. Use of a valved RV-PA shunt prevents diastolic regurgitation from PA to RV, and should further decrease ventricular preload. However, the present theoretical study based on mathematical models revealed that the valved RV-PA shunt mainly improves pulmonary blood supply and the favorable effect on ventricular energetics is equivalent to that of the non-valved RV-PA shunt.

Influence on systemic circulation

In the SPS model, the use of a larger caliber shunt increased systolic SAP and decreased diastolic SAP. In both the valved and non-valved RV-PA shunt models, however, systolic and diastolic SAP did not change with the increase in shunt diameter. Diastolic SAP in both RV-PA shunt models were at most 8 mmHg higher than that in the SPS model. Some clinical reports have already demonstrated lower diastolic SAP using the SPS [18, 19]. Lower diastolic SAP may decrease coronary perfusion

pressure and result in coronary malperfusion. Therefore, excessive decrease in diastolic SAP when using the SPS may cause global myocardial ischemia and impair the postoperative surgical outcome. On the other hand, higher and stable diastolic SAP with both the valved and non-valved RV-PA shunts is favorable for myocardial blood supply.

Influence on pulmonary circulation

The Q_p was excessively high in the SPS model, but was lower in both the valved and non-valved RV-PA shunt models. The Q_p in the 3.5-mm SPS model was similar to that in the 5.0-mm valved RV-PA shunt and higher than that in the 6.0-mm non-valved RV-PA shunt model. The RV-PA shunts contributed to avoiding pulmonary over-circulation and maintaining appropriate pulmonary blood supply in spite of the larger conduits.

In the present study, the valved RV-PA shunt eliminated diastolic regurgitation from PA to RV, and improved pulmonary blood supply compared to the non-valved RV-PA shunt. At the same shunt diameter, Q_p was at most 42% higher in the valved RV-PA shunt than in the non-valved RV-PA shunt model. This resulted in higher oxygen saturation in the valved RV-PA shunt. To obtain the same Q_p as the valved RV-PA shunt, a non-valved RV-PA shunt may require larger stressed blood volume and may cause the increase in ventricular preload. Since some authors reported decreased SvO_2 as a predictor of morbidity after the Norwood procedure [20, 21], the valved RV-PA shunt that yields higher SvO_2 may be favorable for pulmonary circulation.

Caspi et al. [22] suggested that the Norwood procedure with RV-PA conduit may have favorable effects on the development of the pulmonary artery, which may be associated with the pulsatile pulmonary flow. The importance of pulsatility for the growth of pulmonary artery has been reported [23, 24]. The smaller pulsatility of pulmonary flow in the SPS as shown in Fig. 2d may impair the development of the pulmonary artery.

Influence on RVEDV

The RVEDV was markedly reduced in both the non-valved and valved RV-PA shunt models compared to the SPS model. When using a SPS, systemic and pulmonary arteries are directly connected. Therefore, a blood shift from systemic to pulmonary circulation in the diastolic phase (diastolic run-off) cannot be avoided, because pulmonary vascular resistance is usually lower than systemic vascular resistance. This should cause a decrease in systemic arterial pressure and require a greater stressed blood volume to maintain the mean SAP (Table 2), resulting in increased RVEDV and Q_p. When the RV-PA shunts are used, since systemic and pulmonary arteries originate separately from the RV, diastolic run-off is avoided and RVEDV and Q_p are lower as a result. The lower RVEDV contributes to improvement of ventricular energetics as described below.

Influence on ventricular energetics

Diastolic regurgitation from PA to RV occurs when a non-valved RV-PA shunt is used. It is possible that the diastolic regurgitation may increase ventricular preload and impair ventricular energetics compared to the valved RV-PA shunt. However, the present study demonstrated that use of both the valved and non-valved RV-PA shunts eliminated systemic to pulmonary diastolic run-off and improved mechanical efficiency (SW/PVA) to the same extent. Compared to the 3.5-mm SPS model, the lower RVEDV in both the 5.0-mm valved and 6.0 mm non-valved RV-PA shunt models contributed to decreasing PVA (−27.2 and −18.0%, respectively) and increasing mechanical efficiency (+5.3 and +9.2%, respectively). Therefore, the influence of diastolic regurgitation associated with the non-valved RV-PA shunt may be small from the viewpoint of ventricular energetics. Because PVA correlates significantly with myocardial oxygen consumption [24], decreased PVA results in reduced myocardial oxygen demand. The present results suggest that both RV-PA shunts reduce myocardial oxygen demand.

This advantage of both RV-PA shunts in ventricular energetics may be associated with the RV ejection pattern through the RV-PA shunts. With the SPS, RV has to pump the blood to a higher pressure system i.e., the systemic circulation. This limits the duration of RV ejection and requires higher RV systolic pressure. However, with both the RV-PA shunts, the systemic and pulmonary arteries originate separately from the RV. The RV ejects blood steadily via the RV-PA shunt to the pulmonary circulation that has a relatively low pressure (Fig. 2). This fact may contribute to the decreased SW and PVA when using the valved and non-valved RV-PA shunts.

Advantage of RV-PA shunt

The higher diastolic SAP obtained from using a RV-PA shunt has been reported to improve coronary blood supply [1]. However, under physiological conditions, coronary blood flow depends on myocardial oxygen demand [25]. The greatest advantage of the RV-PA shunt is that this procedure decreases myocardial oxygen demand through decreasing PVA. The RV-PA shunt is able to maintain systemic circulation at lower oxygen consumption compared to the SPS, implying that the RV-PA shunt requires less coronary blood flow than the SPS to maintain the same

Table 3 The influence of ventriculotomy on ventricular energetics

	$E_{es,RV}$ (mmHg/ml)	SW (mmHg ml)	PVA (mmHg ml)	Mechanical efficiency (%)
3.5-mm SPS	8.5	905	1,157	78.2
6.0-mm non-valved RV-PA	7.5	827	977	84.7
	6.5	825	1,018	81.1
5.0-mm valved RV-PA	7.5	702	875	80.3
	6.5	698	916	76.2

SPS systemic to pulmonary artery shunt, *RV-PA* right ventricle to pulmonary artery shunt, $E_{es,RV}$ end-systolic elastance of right ventricle, *SW* stroke work, *PVA* systolic pressure–volume area

systemic circulation. This feature may contribute to the improvement of coronary flow reserve. The RV-PA shunt may have better tolerance to the postoperative myocardial ischemia.

Limitations

The present study had some limitations. First, the potential damage of right ventriculotomy was disregarded in the present simulations. Ventricular incision is required to place the valved or non-valved RV-PA shunt. Although ventriculotomy may cause ventricular systolic dysfunction or tricuspid regurgitation, Graham et al. [26] observed no apparent deleterious effects of right ventriculotomy following the Norwood procedure using a RV-PA shunt. Furthermore, our additional simulation suggested that the RV-PA shunt still improved ventricular energetics in spite of the potential damage of ventriculotomy, which decreased the end-systolic elastance of RV ($E_{es,RV}$) from 8.5 to 7.5 mmHg/ml (Table 3). However, mechanical efficiency in the 5.0-mm valved RV-PA shunt would be lower than that in the 3.5-mm SPS when ventriculotomy decreased $E_{es,RV}$ to 6.5 mmHg/ml.

Second, systemic and pulmonary vascular resistance did not change in the present simulations. Vascular resistance was the same in all three shunt models. The differences in pulsatility of the three procedures may affect vascular resistance. A previous report indicated that a sudden increase in systemic vascular resistance caused circulatory collapse in Norwood patients [27]. Therefore, further analyses on the influence of vascular resistance are required.

Third, inertial effects in the shunt were disregarded in the present study. If we considered flow in the shunt as unsteady flow, inertial effects would have a great impact on the pressure-drop across the shunt. [28] Then, the length of shunt might become a strong determinant of pressure–flow relationship.

Conclusions

The present theoretical analysis indicates that both the valved and non-valved RV-PA shunts maintain adequate pulmonary circulation; as a result, the RV delivers greater SW for a lower PVA, i.e., lower myocardial oxygen consumption. Although the valved RV-PA shunt improves pulmonary blood supply and consequently increases Q_p and oxygen saturation compared to the non-valved RV-PA shunt, the favorable effects of the two RV-PA shunts on ventricular energetics are equivalent. The non-valved RV-PA shunt reduces PVA and improves mechanical efficiency in spite of the presence of PA to RV regurgitation.

Acknowledgments This study was supported by a research project promoted by the Japanese Ministry of Health, Labour and Welfare (H20-katsudo-Shitei-007 and H21-nano-Ippan-005); Grants-in-Aid for Scientific Research (No. 20390462, No. 22791328 and No. 23390415) from the Ministry of Education, Culture, Sports, Science and Technology; and the Industrial Technology Research Grant Program from New Energy and Industrial Technology Development Organization (NEDO) of Japan.

References

1. Maher KO, Pizarro C, Gidding SS, Januszewska K, Malec E, Norwood WI Jr, Murphy JD (2003) Hemodynamic profile after the Norwood procedure with right ventricle to pulmonary artery conduit. Circulation 108:782–784
2. Bove EL, Migliavacca F, de Leval MR, Balossino R, Pennati G, Lloyd TR, Khambadkone S, Hsia TY, Dubini G (2008) Use of mathematic modeling to compare and predict hemodynamic effects of the modified Blalock–Taussig and right ventricle-pulmonary artery shunts for hypoplastic left heart syndrome. J Thorac Cardiovasc Surg 136:312–320.e2
3. Reinhartz O, Reddy VM, Petrossian E, MacDonald M, Lamberti JJ, Roth SJ, Wright GE, Perry SB, Suleman S, Hanley FL (2006) Homograft valved right ventricle to pulmonary artery conduit as a modification of the Norwood procedure. Circulation 114:I594–I599
4. Takeuchi K, Murakami A, Takaoka T, Takamoto S (2006) Evaluation of valved saphenous vein homograft as right ventricle-pulmonary artery conduit in modified stage I Norwood operation. Interact Cardiovasc Thorac Surg 5:345–348
5. Burkhoff D, Tyberg JV (1993) Why does pulmonary venous pressure rise after onset of LV dysfunction: a theoretical analysis. Am J Physiol 265:H1819–H1828
6. Morley D, Litwak K, Ferber P, Spence P, Dowling R, Meyns B, Griffith B, Burkhoff D (2007) Hemodynamic effects of partial ventricular support in chronic heart failure: results of simulation validated with in vivo data. J Thorac Cardiovasc Surg 133:21–28
7. Shimizu S, Shishido T, Une D, Kamiya A, Kawada T, Sano S, Sugimachi M (2010) Right ventricular stiffness constant as a predictor of postoperative hemodynamics in patients with

hypoplastic right ventricle: a theoretical analysis. J Physiol Sci 60:205–212
8. Sagawa K, Maughan L, Suga H, Sunagawa K (1988) Cardiovascular interaction. In: Sagawa K, Maughan L, Suga H, Sunagawa K (eds) Cardiac contraction and the pressure–volume relationship. Oxford University Press, Oxford
9. Migliavacca F, Pennati G, Dubini G, Fumero R, Pietrabissa R, Urcelay G, Bove EL, Hsia TY, de Leval MR (2001) Modeling of the Norwood circulation: effects of shunt size, vascular resistances, and heart rate. Am J Physiol Heart Circ Physiol 280:H2076–H2086
10. Huikeshoven F, Coleman TG, Jongsma HW (1980) Mathematical model of the fetal cardiovascular system: the uncontrolled case. Am J Physiol 239:R317–R325
11. Migliavacca F, Dubini G, Pennati G, Pietrabissa R, Fumero R, Hsia TY, de Leval MR (2000) Computational model of the fluid dynamics in systemic-to-pulmonary shunts. J Biomech 33:549–557
12. Young DF, Tsai FY (1973) Flow characteristics in models of arterial stenoses. I. Steady flow. J Biomech 6:395–410
13. Chang AC, Kulik TJ, Hickey PR, Wessel DL (1993) Real-time gas-exchange measurement of oxygen consumption in neonates and infants after cardiac surgery. Crit Care Med 21:1369–1375
14. Norwood WI, Lang P, Hansen DD (1983) Physiologic repair of aortic atresia-hypoplastic left heart syndrome. N Engl J Med 308:23–26
15. Pizarro C, Malec E, Maher KO, Januszewska K, Gidding SS, Murdison KA, Baffa JM, Norwood WI (2003) Right ventricle to pulmonary artery conduit improves outcome after stage I Norwood for hypoplastic left heart syndrome. Circulation 108:II155–II160
16. Sano S, Ishino K, Kawada M, Arai S, Kasahara S, Asai T, Masuda Z, Takeuchi M, Ohtsuki S (2003) Right ventricle-pulmonary artery shunt in first-stage palliation of hypoplastic left heart syndrome. J Thorac Cardiovasc Surg 126:504–509
17. Yamashiro M, Morita K, Uno Y, Shinohara G, Hashimoto K (2011) Modified Norwood procedure with a handmade downsizing valved right ventricle-to-pulmonary artery conduit. Gen Thorac Cardiovasc Surg 59:30–33
18. Bradley SM, Simsic JM, McQuinn TC, Habib DM, Shirali GS, Atz AM (2004) Hemodynamic status after the Norwood procedure: a comparison of right ventricle-to-pulmonary artery connection versus modified Blalock–Taussig shunt. Ann Thorac Surg 78:933–941
19. Azakie A, Martinez D, Sapru A, Fineman J, Teitel D, Karl TR (2004) Impact of right ventricle to pulmonary artery conduit on outcome of the modified Norwood procedure. Ann Thorac Surg 77:1727–1733
20. Hoffman GM, Ghanayem NS, Kampine JM, Berger S, Mussatto KA, Litwin SB, Tweddell JS (2000) Venous saturation and the anaerobic threshold in neonates after the Norwood procedure for hypoplastic left heart syndrome. Ann Thorac Surg 70:1515–1520
21. Hoffman GM, Tweddell JS, Ghanayem NS, Mussatto KA, Stuth EA, Jaquis RD, Berger S (2004) Alteration of the critical arteriovenous oxygen saturation relationship by sustained afterload reduction after the Norwood procedure. J Thorac Cardiovasc Surg 127:738–745
22. Caspi J, Pettitt TW, Mulder T, Stopa A (2008) Development of the pulmonary arteries after the Norwood procedure: comparison between Blalock–Taussig shunt and right ventricular-pulmonary artery conduit. Ann Thorac Surg 86:1299–1304
23. Malec E, Januszewska K, Kolcz J, Mroczek T (2003) Right ventricle-to-pulmonary artery shunt versus modified Blalock–Taussig shunt in the Norwood procedure for hypoplastic left heart syndrome—influence on early and late haemodynamic status. Eur J Cardiothorac Surg 23:728–733
24. Suga H, Yasumura Y, Nozawa T, Futaki S, Igarashi Y, Goto Y (1987) Prospective prediction of O_2 consumption from pressure-volume area in dog hearts. Am J Physiol 252:H1258–H1264
25. Tune JD, Gorman MW, Feigl EO (2004) Matching coronary blood flow to myocardial oxygen consumption. J Appl Physiol 97:404–415
26. Graham EM, Atz AM, Bradley SM, Scheurer MA, Bandisode VM, Laudito A, Shirali GS (2007) Does a ventriculotomy have deleterious effects following palliation in the Norwood procedure using a shunt placed from the right ventricle to the pulmonary arteries? Cardiol Young 17:145–150
27. Wright GE, Crowley DC, Charpie JR, Ohye RG, Bove EL, Kulik TJ (2004) High systemic vascular resistance and sudden cardiovascular collapse in recovering Norwood patients. Ann Thorac Surg 77:48–52
28. Young DF, Tsai FY (1973) Flow characteristics in models of arterial stenoses. II. Unsteady flow. J Biomech 6:547–559

Autonomic Neuroscience: Basic and Clinical 162 (2011) 60–65

Contents lists available at ScienceDirect

Autonomic Neuroscience: Basic and Clinical

journal homepage: www.elsevier.com/locate/autneu

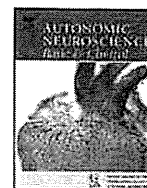

Centrally administered ghrelin activates cardiac vagal nerve in anesthetized rabbits

Shuji Shimizu [a,b,*], Tsuyoshi Akiyama [a], Toru Kawada [a], Takashi Sonobe [a], Atsunori Kamiya [a], Toshiaki Shishido [a], Takeshi Tokudome [a], Hiroshi Hosoda [a], Mikiyasu Shirai [a], Kenji Kangawa [a], Masaru Sugimachi [a]

[a] National Cerebral and Cardiovascular Center Research Institute, Osaka, Japan
[b] Japan Association for the Advancement of Medical Equipment, Tokyo, Japan

ARTICLE INFO

Article history:
Received 30 June 2010
Received in revised form 8 March 2011
Accepted 6 April 2011

Keywords:
Ghrelin
Cardiac microdialysis
Norepinephrine
Acetylcholine
Vagal nerve

ABSTRACT

Although central ghrelin has cardioprotective effect through inhibiting sympathetic nerve activity, the effects of central ghrelin on cardiac vagal nerve remain unknown. We investigated the effects of centrally administered ghrelin on cardiac autonomic nerve activities using microdialysis technique. A microdialysis probe was implanted in the right atrial wall adjacent to the sinoatrial node of an anesthetized rabbit and was perfused with Ringer's solution containing a cholinesterase inhibitor, eserine. After injection of ghrelin (1 nmol) into the right lateral cerebral ventricle, norepinephrine (NE) and acetylcholine (ACh) concentrations in the dialysate samples were measured as indices of NE and ACh release from nerve endings to the sinoatrial node using high-performance liquid chromatography. Heart rate was 270 ± 4 bpm at baseline and decreased gradually after ghrelin injection to 234 ± 9 bpm ($P<0.01$) at 60–80 min, followed by gradual recovery. Dialysate ACh concentration was 5.5 ± 0.8 nM at baseline and increased gradually after ghrelin injection to 8.8 ± 1.2 nM ($P<0.01$) at 60–80 min; the concentration started to decrease gradually from 100 to 120 min after injection reaching 5.6 ± 0.8 nM at 160–180 min. Central ghrelin did not change mean arterial pressure or dialysate NE concentration. The elevated dialysate ACh concentration declined rapidly after transection of cervical vagal nerves. These results indicate that centrally administered ghrelin activates cardiac vagal nerve.
© 2011 Elsevier B.V. All rights reserved.

1. Introduction

Ghrelin, a growth-hormone-releasing acylated peptide, was originally isolated from rat stomach (Kojima et al., 1999). Immunohistochemical studies have revealed that ghrelin-immunoreactive neurons are also present in the central nervous system including the hypothalamic arcuate nucleus (ARC) (Date et al., 2000) and that growth hormone secretagogue receptors (GHS-R) are expressed in hypothalamic nucleus including the ARC (Guan et al., 1997). Several studies have demonstrated that centrally administered ghrelin inhibits sympathetic nerve activity. Matsumura et al. (2002) reported that intracerebroventricular (icv) injection of ghrelin decreased renal sympathetic nerve activity in conscious rabbits. Lin et al. (2004) showed that microinjection of ghrelin into the nucleus of the solitary tract (NTS) also suppressed the renal sympathetic nerve activity in rats. However, whether central ghrelin affects cardiac vagal nerve activity remains unknown. Recently we have developed a microdialysis technique that allows direct monitoring of norepinephrine (NE) and acetylcholine (ACh) released into the sinoatrial (SA) node (Shimizu et al., 2009, 2010). Dialysate NE or ACh concentration monitored by this technique significantly correlates with heart rate and the frequencies of electrical stimulation of sympathetic or vagal nerve. In the present study, we used this technique to investigate the effect of centrally administered ghrelin on cardiac vagal nerve activity as well as sympathetic nerve activity in anesthetized rabbits.

2. Materials and Methods

2.1. Surgical Preparation

Animal care was provided in accordance with the *Guiding Principles for the Care and Use of Animals in the Field of Physiological Sciences* approved by the Physiological Society of Japan. All protocols were approved by the Animal Subject Committee of the National Cerebral and Cardiovascular Center. Twenty four Japanese white rabbits weighing 2.3 to 3.1 kg were used in this study. Anesthesia was initiated by an intravenous injection of pentobarbital sodium (50 mg/kg) via the marginal ear vein, and then maintained at an appropriate level by continuous intravenous infusion of α-chloralose (16 mg/kg/h) and urethane (100 mg/kg/h) through a catheter inserted into the femoral vein. Since the duration of this experiment was projected to be over 8 h, the animals were intubated and ventilated mechanically with room air mixed with oxygen. Respiratory rate and tidal volume were set at

* Corresponding author at: Department of Cardiovascular Dynamics, National Cerebral and Cardiovascular Center Research Institute, 5-7-1 Fujishiro-dai, Suita, Osaka 565-8565, Japan. Tel.: +81 6 6833 5012; fax: +81 6 6835 5403.
E-mail address: shujismz@ri.ncvc.go.jp (S. Shimizu).

1566-0702/$ – see front matter © 2011 Elsevier B.V. All rights reserved.
doi:10.1016/j.autneu.2011.04.001

30 cycles/min and 15 ml/kg, respectively. Systemic arterial pressure was monitored by a catheter inserted into the femoral artery. Body temperature was measured in the esophagus by a thermometer (CTM-303, Terumo, Japan), and was maintained between 38 and 39 °C using a heating pad. For icv injection of ghrelin, a polyethylene tube (500 μm outer diameter) was stereotactically inserted into the right lateral cerebral ventricle using a guiding needle (900 μm outer diameter, 600 μm inner diameter) and was perfused continuously with artificial cerebrospinal fluid (CSF) solution (ARTCEREB®, Otsuka, Japan) at a rate of 2 μl/min using a microinjection pump (CMA/102, Carnegie Medicin, Sweden).

With the animal in the lateral position, right lateral thoracotomy was performed and the right 3rd to 5th ribs were partially resected to expose the heart. Three stainless electrodes were placed around the thoracotomy incision to record the body surface electrocardiogram. The heart rate was determined from the electrocardiogram using a cardiotachometer. Heparin sodium (100 IU/kg) was administered intravenously to prevent blood coagulation. A dialysis probe was implanted and dialysis was conducted as described in *Dialysis Technique* below. At the end of the experiment, the animal was euthanized by injecting an overdose of pentobarbital sodium. In the postmortem examination, the right atrial wall with the implanted dialysis fiber was resected. The endocardial side of atrial wall was examined macroscopically to confirm that the dialysis membrane was not exposed to the right atrial lumen.

2.2. Dialysis Technique

The materials and properties of the dialysis probe have been described previously (Akiyama et al., 1991; Shimizu et al., 2009, 2010). A dialysis fiber composed of semipermeable membrane (4 mm length, 310 μm outer diameter, 200 μm inner diameter; PAN-1200, 50,000 molecular weight cutoff; Asahi Chemical, Tokyo, Japan) was attached at both ends to polyethylene tubes (25 cm length, 500 μm outer diameter, 200 μm inner diameter). A fine guiding needle (30 mm length, 510 μm outer diameter, 250 μm inner diameter) with a stainless steel rod (5 mm length, 250 μm outer diameter) was used for implantation. A dialysis probe was implanted into the right atrial myocardium near the junction between the superior vena cava and the right atrium. After implantation, the dialysis probe was perfused with Ringer's solution (NaCl 147 mM, KCl 4 mM, and $CaCl_2$ 3 mM) containing the cholinesterase inhibitor, eserine (100 μM), at a rate of 2 μl/min using a microinjection pump (CMA/102). Experimental protocols were started 120 min after implantation of the dialysis probe. We took account of the dead space between the dialysis membrane and the sample tube at the start of each dialysate sampling. Eight microliters of phosphate buffer (pH 3.5) was added to each sample tube before dialysate sampling. The duration of dialysate sampling was fixed at 20 min (1 sample volume = 40 μl). Half of the dialysate sample was used for ACh measurement and the other half for NE. Dialysate NE and ACh concentrations were measured separately using two high-performance liquid chromatographs with electrochemical detection as previously described (Akiyama et al., 1991, 1994).

2.3. Experimental Protocols

2.3.1. Protocol 1

We investigated the time courses of heart rate, mean arterial pressure, and dialysate NE and ACh concentrations following icv injection of ghrelin. One hundred microliters of artificial CSF containing 1 nmol of human ghrelin (Peptide Institute, Osaka, Japan) or 100 μl of artificial CSF alone (vehicle) was injected into the lateral cerebral ventricle of a rabbit. Baseline dialysate sample was collected before injection and then 20-min dialysate samples were collected consecutively up to 180 min after injection.

2.3.2. Protocol 2

We investigated the effect of vagotomy on heart rate and cardiac vagal ACh release after icv injection of ghrelin (1 nmol). Baseline dialysate sample was collected before icv injection of ghrelin and another sample was collected when heart rate reached a trough after ghrelin injection. Immediately after this sampling, bilateral cervical vagal nerves were transected and dialysate was sampled for a 20-min duration.

2.3.3. Protocol 3

As a supplemental protocol, we investigated the dose-dependent effects of ghrelin on heart rate and dialysate ACh concentration using icv injection of 0.2 nmol ($n=3$) or 5 nmol ($n=4$) of human ghrelin into the right lateral cerebral ventricle. Baseline dialysate sample was collected before injection and then 20-min dialysate samples were collected consecutively up to 180 min after injection.

2.4. Statistical analysis

Heart rate and mean arterial pressure were averaged over each 20-min duration of dialysate sampling. All data are presented as mean ± SE. In Protocols 1 and 2, heart rate and mean arterial pressure were compared by one-way repeated measures analysis of variance (ANOVA) followed by a Dunnett's test against baseline. Our previous studies demonstrated that dialysate NE or ACh concentration exponentially increased in response to electrical stimulation of sympathetic or vagal nerve. Then, heart rate linearly correlated with logarithms of dialysate NE or ACh concentration (Shimizu et al., 2009, 2010). Thus, after logarithmic transformation, dialysate NE and ACh concentrations were compared by one-way repeated measures ANOVA followed by a Dunnett's test against baseline. The differences between ghrelin and vehicle groups were compared using unpaired *t*-test. Differences were considered significant at $P<0.05$.

3. Results

3.1. Protocol 1

In the ghrelin-treated rabbits, the heart rate was 270 ± 4 bpm at baseline and decreased gradually after icv ghrelin injection reaching a trough of 233 ± 9 bpm at 80–100 min ($P<0.01$ vs. baseline), followed by gradual recovery (271 ± 8 bpm at 160–180 min). In the vehicle control group, heart rate was 270 ± 6 bpm at baseline and increased slightly to 278 ± 6 bpm at 40–60 min after injection ($P<0.05$ vs. baseline), and was maintained until the end of the protocol (284 ± 7 bpm at the 160–180 min, $P<0.01$ vs. baseline) (Fig. 1A).

Although mean arterial pressure did not change after icv injection of ghrelin and remained constant throughout the experiment, mean arterial pressure decreased gradually from 80 ± 4 mm Hg at baseline to 72 ± 2 mm Hg at 160–180 min ($P<0.01$ vs. baseline) after icv injection of vehicle (Fig. 1B).

Dialysate ACh concentration did not change after icv injection of vehicle. In the ghrelin-treated rabbits, the dialysate ACh concentration was 5.5 ± 0.8 nM at baseline and increased gradually after ghrelin injection, reaching a plateau of 8.8 ± 1.2 nM at 60–80 min ($P<0.01$ vs. baseline). The concentration appeared to decline after 100 min and returned to 5.6 ± 0.8 nM at 160–180 min (N.S. vs. baseline) (Fig. 2A).

Dialysate NE concentration did not change after icv injection of ghrelin or vehicle, and did not vary significantly throughout the experiment (Fig. 2B).

3.2. Protocol 2

Heart rate decreased significantly from 283 ± 5 bpm at baseline to a trough of 249 ± 5 bpm after icv injection of ghrelin ($P<0.01$ vs. baseline) (Table 1). Dialysate ACh concentration increased from 5.3 ± 1.3 nM at

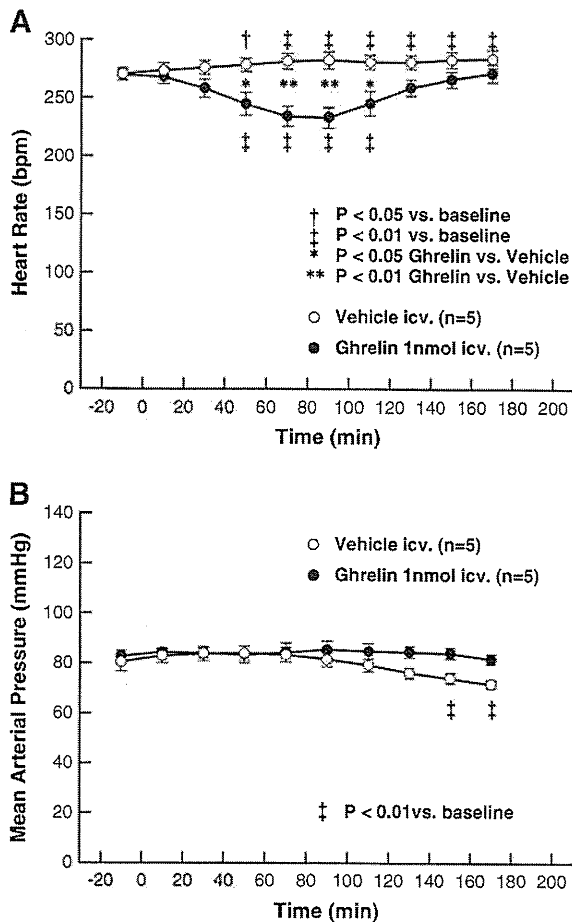

Fig. 1. Time courses of heart rate (A) and mean arterial pressure (B) elicited by intracerebroventricular (icv) injection of 1 nmol of ghrelin (●) or artificial cerebrospinal fluid (vehicle, ○) (n = 5 in each group). Data are presented as values averaged over each 20-min duration of dialysate sampling. Values are mean ± SE. † P<0.05, ‡ P<0.01 vs. baseline before injection by one-way repeated measures analysis of variance followed by Dunnett's test. * P<0.05, ** P<0.01 ghrelin vs. vehicle by unpaired *t*-test.

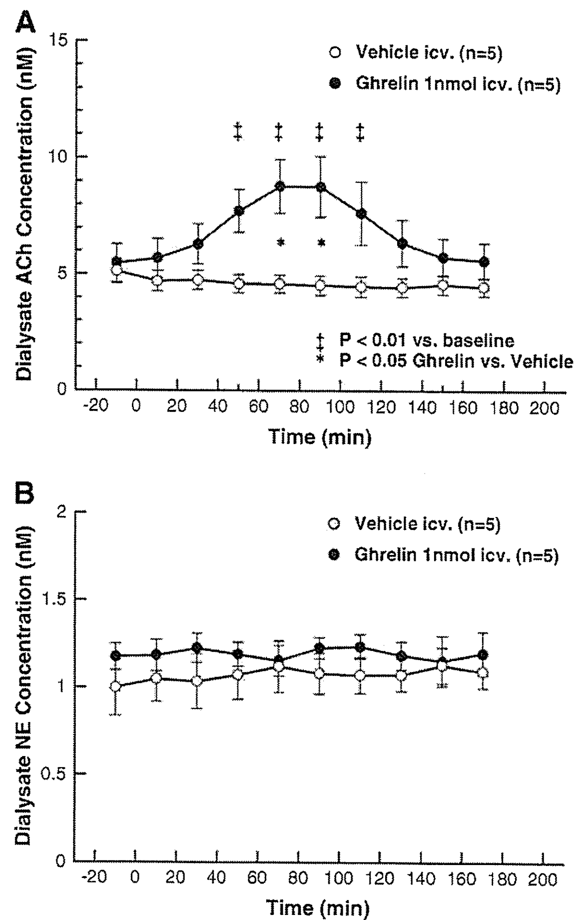

Fig. 2. Time courses of dialysate acetylcholine (ACh) (A) and norepinephrine (NE) (B) concentrations elicited by icv injection of ghrelin (●) or vehicle (○) (n = 5 in each group). Data are concentrations in dialysate samples collected over 20-min durations. Values are mean ± SE. Statistical comparison was performed after logarithmic transformation. ‡ P<0.01 vs. baseline before injection by one-way repeated measures analysis of variance followed by Dunnett's test. * P<0.05, ghrelin vs. vehicle by unpaired *t*-test.

baseline to 9.5 ± 2.2 nM at the time of trough heart rate after icv ghrelin injection (P<0.01 vs. baseline) (Fig. 3A). After vagotomy, heart rate immediately increased to 286 ± 8 bpm (N.S. vs. baseline) and mean arterial pressure decreased to 76 ± 9 mm Hg (P<0.05 vs. baseline), while dialysate ACh concentration recovered to the baseline level (6.6 ± 1.9 nM, N.S. vs. baseline). Typical heart rate response after vagotomy is shown in Fig. 3B.

3.3. Protocol 3

Heart rate decreased from 272 ± 15 bpm at baseline to 209 ± 29 bpm at 80–100 min after icv injection of 5 nmol of ghrelin (Fig. 4A). Dialysate ACh concentration increased from 6.4 ± 1.2 nM at baseline to 11.2 ± 1.7 nM at 80–100 min after icv injection of 5 nmol of ghrelin (Fig. 4B). At the end of this experiment, heart rate was still lower (224 ± 23 bpm) than the baseline heart rate and dialysate ACh concentration was still higher (9.1 ± 0.9 nM) than that of baseline. Statistical analysis on these data was avoided due to the limited number of animals in the supplemental protocol.

Heart rate and dialysate ACh concentration did not change perceivably after icv injection of 0.2 nmol of ghrelin (Fig. 4A and B).

4. Discussion

The major finding of the present study is that centrally administered ghrelin increases ACh release into the SA node by activating efferent cardiac vagal nerves.

4.1. Ghrelin and cardiac vagal nerve activity

Intracerebroventricular injection of ghrelin is known to activate efferent vagal nerves in digestive organs. Li et al. (2006) and Sato et al. (2003) have

Table 1
Changes in heart rate and mean arterial pressure after intracerebroventricular injection of 1 nmol of ghrelin followed by vagotomy.

	Heart rate (bpm)	Mean arterial pressure (mm Hg)
Baseline (before injection)	283 ± 5	82 ± 7
Trough level after injection (before vagotomy)	249 ± 5**	79 ± 8
After vagotomy	286 ± 8	76 ± 9*

Values are mean ± SE (n = 7).
* P<0.05 vs. baseline.
** P<0.01 vs. baseline.

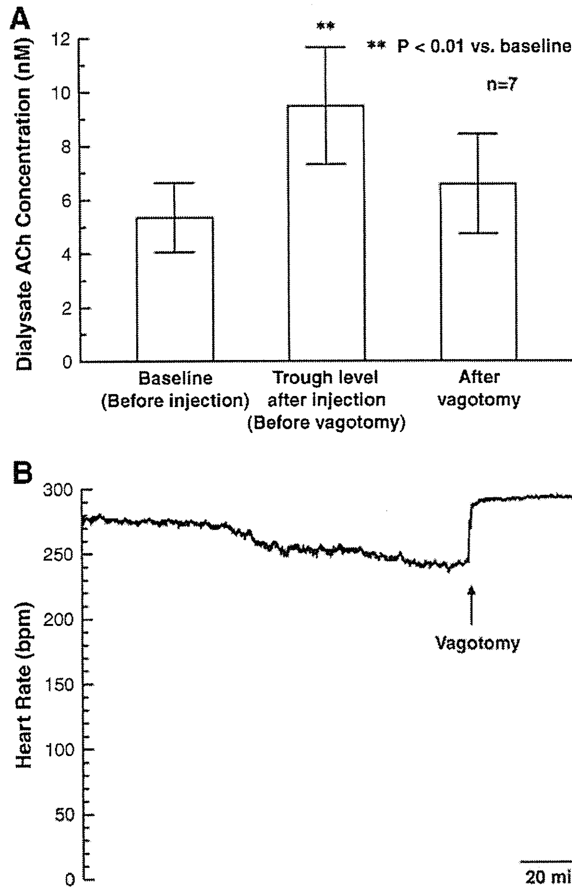

Fig. 3. A: Effect of vagotomy after icv injection of 1 nmol of ghrelin on dialysate ACh concentration (n = 7). Values are mean ± SE. Statistical comparison was performed after logarithmic transformation. ** P<0.01 vs. baseline before injection by one-way repeated measures analysis of variance followed by Dunnett's test. B: Typical time course of heart rate change. Heart rate gradually decreased after icv injection of ghrelin and promptly returned to the baseline level after vagatomy.

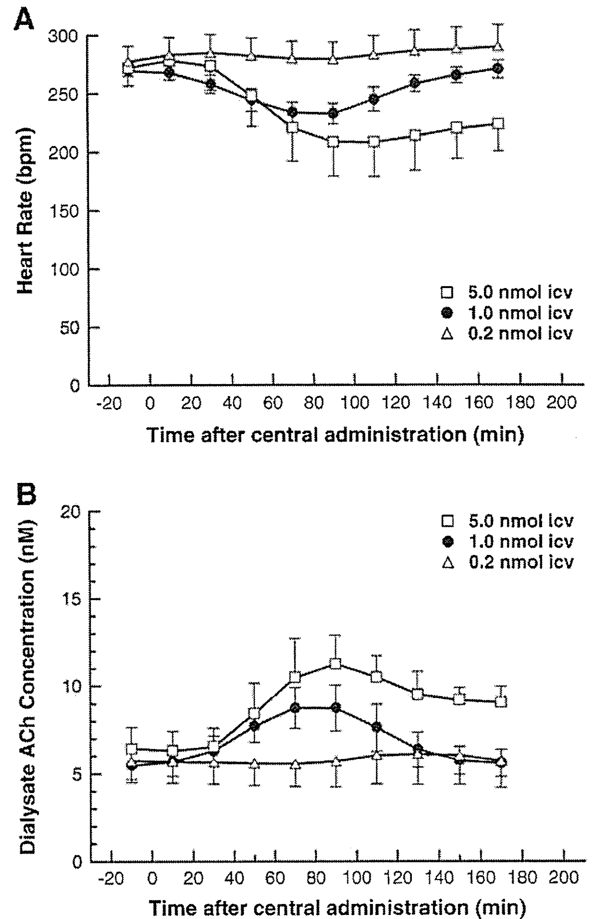

Fig. 4. Time courses of heart rate (A) and dialysate ACh concentration (B) elicited by icv injection of 0.2 nmol (△, n = 3) or 5 nmol (□, n = 4) of ghrelin. Graphs of icv injection of 1 nmol of ghrelin (●) were reproduced from Figs. 1A and 2A for intuitive comparison.

demonstrated that icv injection of ghrelin stimulates pancreatic secretion by activating efferent vagal nerves. Kobashi et al. (2009) have shown that icv injection of ghrelin induces relaxation of the proximal stomach through activation of efferent vagal nerves. Vagal nerves also play an important role in the regulation of heart rate under physiological conditions. Moreover, vagal stimulation has cardioprotective effect against chronic heart failure (Li et al., 2004; Schwartz et al., 2008). However, the effect of icv injection of ghrelin on cardiac vagal nerve activity has not been reported.

In the present study, icv injection of ghrelin decreased heart rate without affecting mean arterial pressure, and simultaneously increased dialysate ACh concentration without changing dialysate NE concentration. The time course of heart rate changes parallels that of dialysate ACh concentration changes throughout the experiment. Furthermore, dialysate ACh concentration and heart rate recovered to the baseline levels immediately after vagotomy. Thus, the decrease in heart rate by central ghrelin could be due to cardiac vagal activation and not cardiac sympathetic suppression. The present study demonstrates that centrally administered ghrelin activates cardiac vagal nerve and decreases heart rate. The maximal dialysate ACh concentration following icv injection of ghrelin reached 8.8 ± 1.2 nM. This dialysate ACh concentration is almost equivalent to that induced by electrical stimulation of the right cervical vagal nerve at 10–20 Hz (Shimizu et al., 2009). Therefore, ghrelin may be one of the most important mediators in the central nerve system, which activates cardiac vagal nerve.

Ghrelin receptors are present in the central nerve system. In a c-Fos expression study, Date et al. (2001) reported that central ghrelin activated the NTS and dorsal motor nucleus of the vagus (DMNV). Zigman et al. (2006) demonstrated the presence of GHS-R in all three divisions of the dorsal vagal complex using in situ hybridization. The GHS-Rs are also expressed in the hypothalamus including the ARC (Guan et al., 1997). Central administration of ghrelin may activate cardiac vagal nerve through direct action on central ghrelin receptors, although it is difficult to determine the brain region in which ghrelin acts from the present study.

There was a long time lag between icv injection of ghrelin and activation of the cardiac vagal nerve. This may suggest that other mediators are involved in ghrelin-induced activation of cardiac vagal nerve. Intracerebroventricular injection of ghrelin evokes growth hormone release (Date et al., 2000). Resmini et al. (2006) reported sympathovagal imbalance due to vagal hypertone in acromegalic patients. Sato et al. (2003), however, suggested that the stimulatory effect of ghrelin on pancreatic secretion may be induced independent of its growth-hormone releasing effect, because a maximal increase in growth hormone was observed 10–20 min after ghrelin injection but a peak increase in pancreatic secretion was found 30–60 min after injection. In the present study, the maximal decrease in heart rate (234 ± 9 and 233 ± 9 bpm) and maximal increase in dialysate ACh concentration (8.8 ± 1.2 and 8.7 ± 1.3 nM) were both observed during 60–100 min after icv ghrelin injection. Moreover, Bisi et al. (1999) reported that intravenous administration of recombinant human growth hormone increased circulating growth hormone levels but did

not affect heart rate or mean arterial pressure in humans. Therefore, the stimulatory effect of ghrelin on the cardiac vagal nerve may be independent of its growth hormone releasing effect.

Nakazato et al. (2001) reported that antibodies and antagonists of neuropeptide Y and agouti-related protein abolished ghrelin-enhanced feeding. Kamegai et al. (2001) reported that chronic icv infusion of ghrelin increased both neuropeptide Y and agouti-related protein mRNA levels in the ARC. Moreover, Kobashi et al. (2006) showed that central neuropeptide Y induced proximal stomach relaxation via Y1 receptors in the dorsal vagal complex of rats. Thus, neuropeptide Y and agouti-related protein may be involved in the stimulatory effect of ghrelin on cardiac vagal nerve. However, we need further investigations to identify the mediators involved in the ghrelin-induced cardiac vagal activation.

4.2. Ghrelin and cardiac sympathetic nerve activity

In the present study, icv injection of ghrelin did not change dialysate NE concentration. This result indicates that centrally administered ghrelin did not affect NE release into the SA node under the present experimental conditions. Central ghrelin has been shown to inhibit sympathetic nerve activity in conscious rabbits (Matsumura et al., 2002). The present study was performed under anesthetized conditions. The difference in effect on sympathetic nerve activity may be related to experimental conditions including anesthesia and artificial ventilation. Schwenke et al. (2008) reported that subcutaneous administration of ghrelin prevented the increase in cardiac sympathetic nerve activity in the acute phase after myocardial infarction. Soeki et al. (2008) also reported that sympathetic nerve activity was inhibited by subcutaneous administration of ghrelin in rats with myocardial infarction, but not in sham-operated rats. Ghrelin seems to have a stronger inhibitory effect on the activated sympathetic nervous system than on the non-activated system. The basal sympathetic tone under our experimental conditions may not have been sufficiently high to reveal the sympathoinhibitory effect of ghrelin.

The basal vagal tone could also affect the sympathoinhibitory effect of ghrelin. Lin et al. (2004) reported that microinjection of ghrelin into the NTS did not affect heart rate and reduced the response of mean arterial pressure after intravenous administration of atropine sulfate. Thus, the vagal nerve may play an important role in ghrelin-induced sympathetic suppression. The sympathoinhibitory effect of ghrelin may be partly dependent on prejunctional inhibition of NE release via muscarinic receptors associated with vagal nerve activation. In Lin's study, however, depressor response of ghrelin appeared even after atropine treatment. Thus, it is highly possible that centrally administered ghrelin has a certain sympathoinhibitory effect. We need further investigations about the sympathoinhibitory effect of ghrelin.

4.3. Methodological considerations

First, ACh is degraded by ACh esterase immediately after its release. To monitor ACh release in vivo, addition of an ACh esterase inhibitor (eserine) into the perfusate is required. In our previous study, dialysate ACh concentration correlated well with heart rate and the frequency of cervical vagal nerve stimulation in the presence of eserine (Shimizu et al., 2009). Therefore, the increase in dialysate ACh concentration by icv injection of ghrelin should reflect the activation of cardiac vagal nerve even in the presence of eserine.

Second, the eserine can also affect NE release from sympathetic nerve endings as follows. The eserine should spread around the semipermeable membrane, thereby affecting the NE release in the vicinity of the semipermeable membrane through the enhancement of muscarinic receptor mediated prejunctional inhibition.

Third, to detect changes in dialysate NE and ACh concentration sampled from the right atrium, cardiac microdialysis technique requires 20-min sampling duration. The temporal resolution may be still insufficient compared to acute changes in hemodynamics such as that observed after vagotomy in Protocol 2. The improvement of sensitivity of liquid chromatography will lead to higher temporal resolution of this technique.

Fourth, in the present study, animals were in the supine position during dialysate sampling because this experiment was performed at open-chest condition for cardiac microdialysis. The supine position may have delayed the diffusion of ghrelin and prolonged the time-lag between the injection and vagal nerve activation. Thus, the position of animals may affect the time course of hemodynamics.

4.4. Conclusion

Using cardiac microdialysis technique, we demonstrated that centrally administered ghrelin was able to activate cardiac vagal nerve. Central ghrelin may play an important role in vagal cardiovascular control.

Acknowledgments

This study was supported by the research project promoted by Ministry of Health, Labour and Welfare in Japan (H20-katsudo-Shitei-007, H21-nano-ippan-005), the Grants-in-Aid for Scientific Research promoted by Ministry of Education, Culture, Sports, Science and Technology in Japan (#20390462 and #20590242) and the Industrial Technology Research Grant Program from New Energy and Industrial Technology Development Organization (NEDO) of Japan.

References

Akiyama, T., Yamazaki, T., Ninomiya, I., 1991. In vivo monitoring of myocardial interstitial norepinephrine by dialysis technique. Am. J. Physiol. 261, H1643–H1647.

Akiyama, T., Yamazaki, T., Ninomiya, I., 1994. In vivo detection of endogenous acetylcholine release in cat ventricles. Am. J. Physiol. 266, H854–H860.

Bisi, G., Podio, V., Valetto, M.R., Broglio, F., Bertuccio, G., Del Rio, G., Arvat, E., Boghen, M.F., Deghenghi, R., Muccioli, G., Ong, H., Ghigo, E., 1999. Acute cardiovascular and hormonal effects of GH and hexarelin, a synthetic GH-releasing peptide, in humans. J. Endocrinol. Invest. 22, 266–272.

Date, Y., Murakami, N., Kojima, M., Kuroiwa, T., Matsukura, S., Kangawa, K., Nakazato, M., 2000. Central effects of a novel acylated peptide, ghrelin, on growth hormone release in rats. Biochem. Biophys. Res. Commun. 275, 477–480.

Date, Y., Nakazato, M., Murakami, N., Kojima, M., Kangawa, K., Matsukura, S., 2001. Ghrelin acts in the central nervous system to stimulate gastric acid secretion. Biochem. Biophys. Res. Commun. 280, 904–907.

Guan, X.M., Yu, H., Palyha, O.C., McKee, K.K., Feighner, S.D., Sirinathsinghji, D.J., Smith, R.G., Van der Ploeg, L.H., Howard, A.D., 1997. Distribution of mRNA encoding the growth hormone secretagogue receptor in brain and peripheral tissues. Brain Res. Mol. Brain Res. 48, 23–29.

Kamegai, J., Tamura, H., Shimizu, T., Ishii, S., Sugihara, H., Wakabayashi, I., 2001. Chronic central infusion of ghrelin increases hypothalamic neuropeptide Y and Agouti-related protein mRNA levels and body weight in rats. Diabetes 50, 2438–2443.

Kobashi, M., Shimatani, Y., Shirota, K., Xuan, S.Y., Mitoh, Y., Matsuo, R., 2006. Central neuropeptide Y induces proximal stomach relaxation via Y1 receptors in the dorsal vagal complex of the rat. Am. J. Physiol. Regul. Integr. Comp. Physiol. 290, R290–R297.

Kobashi, M., Yanagihara, M., Fujita, M., Mitoh, Y., Matsuo, R., 2009. Fourth ventricular administration of ghrelin induces relaxation of the proximal stomach in the rat. Am. J. Physiol. Regul. Integr. Comp. Physiol. 296, R217–R223.

Kojima, M., Hosoda, H., Date, Y., Nakazato, M., Matsuo, H., Kangawa, K., 1999. Ghrelin is a growth-hormone-releasing acylated peptide from stomach. Nature 402, 656–660.

Li, M., Zheng, C., Sato, T., Kawada, T., Sugimachi, M., Sunagawa, K., 2004. Vagal nerve stimulation markedly improves long-term survival after chronic heart failure in rats. Circulation 109, 120–124.

Li, Y., Wu, X., Zhao, Y., Chen, S., Owyang, C., 2006. Ghrelin acts on the dorsal vagal complex to stimulate pancreatic protein secretion. Am. J. Physiol. Gastrointest. Liver Physiol. 290, G1350–G1358.

Lin, Y., Matsumura, K., Fukuhara, M., Kagiyama, S., Fujii, K., Iida, M., 2004. Ghrelin acts at the nucleus of the solitary tract to decrease arterial pressure in rats. Hypertension 43, 977–982.

Matsumura, K., Tsuchihashi, T., Fujii, K., Abe, I., Iida, M., 2002. Central ghrelin modulates sympathetic activity in conscious rabbits. Hypertension 40, 694–699.

Nakazato, M., Murakami, N., Date, Y., Kojima, M., Matsuo, H., Kangawa, K., Matsukura, S., 2001. A role for ghrelin in the central regulation of feeding. Nature 409, 194–198.

Resmini, E., Casu, M., Patrone, V., Murialdo, G., Bianchi, F., Giusti, M., Ferone, D., Minuto, F., 2006. Sympathovagal imbalance in acromegalic patients. J. Clin. Endocrinol. Metab. 91, 115–120.

Sato, N., Kanai, S., Takano, S., Kurosawa, M., Funakoshi, A., Miyasaka, K., 2003. Central administration of ghrelin stimulates pancreatic exocrine secretion via the vagus in conscious rats. Jpn. J. Physiol. 53, 443–449.
Schwartz, P.J., De Ferrari, G.M., Sanzo, A., Landolina, M., Rordorf, R., Raineri, C., Campana, C., Revera, M., Ajmone-Marsan, N., Tavazzi, L., Odero, A., 2008. Long term vagal stimulation in patients with advanced heart failure: first experience in man. Eur. J. Heart Fail. 10, 884–891.
Schwenke, D.O., Tokudome, T., Kishimoto, I., Horio, T., Shirai, M., Cragg, P.A., Kangawa, K., 2008. Early ghrelin treatment after myocardial infarction prevents an increase in cardiac sympathetic tone and reduces mortality. Endocrinology 149, 5172–5176.
Shimizu, S., Akiyama, T., Kawada, T., Shishido, T., Yamazaki, T., Kamiya, A., Mizuno, M., Sano, S., Sugimachi, M., 2009. In vivo direct monitoring of vagal acetylcholine release to the sinoatrial node. Auton. Neurosci. 148, 44–49.
Shimizu, S., Akiyama, T., Kawada, T., Shishido, T., Mizuno, M., Kamiya, A., Yamazaki, T., Sano, S., Sugimachi, M., 2010. In vivo direct monitoring of interstitial norepinephrine levels at the sinoatrial node. Auton. Neurosci. 152, 115–118.
Soeki, T., Kishimoto, I., Schwenke, D.O., Tokudome, T., Horio, T., Yoshida, M., Hosoda, H., Kangawa, K., 2008. Ghrelin suppresses cardiac sympathetic activity and prevents early left ventricular remodeling in rats with myocardial infarction. Am. J. Physiol. Heart Circ. Physiol. 294, H426–H432.
Zigman, J.M., Jones, J.E., Lee, C.E., Saper, C.B., Elmquist, J.K., 2006. Expression of ghrelin receptor mRNA in the rat and the mouse brain. J. Comp. Neurol. 494, 528–548.

Hindawi Publishing Corporation
Journal of Drug Delivery
Volume 2011, Article ID 453619, 8 pages
doi:10.1155/2011/453619

Research Article

Cellular Injury of Cardiomyocytes during Hepatocyte Growth Factor Gene Transfection with Ultrasound-Triggered Bubble Liposome Destruction

Kazuo Komamura,[1] Rie Tatsumi,[1] Yuko Tsujita-Kuroda,[1] Takatoshi Onoe,[2] Kunio Matsumoto,[3] Toshikazu Nakamura,[3] Jun-ichi Miyazaki,[4] Takeshi Horio,[5] and Masaru Sugimachi[1]

[1] *Department of Cardiovascular Dynamics, Research Institute, National Cerebral and Cardiovascular Center, 5-7-1 Fujishiro-dai, Suita, Osaka 565-8565, Japan*
[2] *Department of Nursing Science, Taisei Gakuin University, Sakai 587-8555, Japan*
[3] *Division of Molecular Regenerative Medicine, Department of Biochemistry and Molecular Biology, Osaka University Graduate School of Medicine, Suita 565-0871, Japan*
[4] *Division of Stem Cell Regulation Research, G6, Osaka University School of Medicine, Suita 565-0871, Japan*
[5] *Division of Hypertension, National Cerebral and Cardiovascular Center, Suita 565-8565, Japan*

Correspondence should be addressed to Kazuo Komamura, kkoma@hsp.ncvc.go.jp

Received 6 August 2010; Accepted 31 October 2010

Academic Editor: Hasan Uludağ

Copyright © 2011 Kazuo Komamura et al. This is an open access article distributed under the Creative Commons Attribution License, which permits unrestricted use, distribution, and reproduction in any medium, provided the original work is properly cited.

We transfected naked HGF plasmid DNA into cultured cardiomyocytes using a sonoporation method consisting of ultrasound-triggered bubble liposome destruction. We examined the effects on transfection efficiency of three concentrations of bubble liposome (1×10^6, 1×10^7, 1×10^8/mL), three concentrations of HGF DNA (60, 120, 180 μg/mL), two insonification times (30, 60 sec), and three incubation times (15, 60, 120 min). We found that low concentrations of bubble liposome and low concentrations of DNA provided the largest amount of the HGF protein expression by the sonoporated cardiomyocytes. Variation of insonification and incubation times did not affect the amount of product. Following insonification, cardiomyocytes showed cellular injury, as determined by a dye exclusion test. The extent of injury was most severe with the highest concentration of bubble liposome. In conclusion, there are some trade-offs between gene transfection efficiency and cellular injury using ultrasound-triggered bubble liposome destruction as a method for gene transfection.

1. Introduction

Ultrasound-triggered bubble liposome destruction (sonoporation) has been proposed as a safe nonviral means of gene therapy that can target many different cells or tissues. In the field of cardiovascular medicine, this method may have significant potential for the introduction of therapeutic genes directly into vascular cells or cardiomyocytes [1, 2]. Sonoporation can only be clinically effective if the dose-effect relationship between the amount of bubble liposome and transfection efficiency is first established. However, few reports have already examined this dose-effect relationship and the safety of the procedure [3].

Transfection efficiency in sonoporation depends on various conditions including type of microbubble, mode of ultrasound, frequency of ultrasound, intensity of acoustic pressure, concentration of microbubble, dose of DNA, duration of insonification, incubation time of cell with DNA, repeat count of insonification, type of targeted cell, and other physicochemical conditions like temperature and carbon dioxide concentration, [3]. Greenleaf et al. reported that ultrasound acoustic pressure, DNA concentration, and

repeat count of insonification correlated with transfection rate [4]. Teupe et al. demonstrated that duration of insonification did not affect transfection rate [5]. Then, Chen et al. showed that transfection rate reached plateau when DNA concentration was increased [6].

Greenleaf et al. also showed that transfection rate peaked and fell off according to the change in liposome concentration [4]. They thought it might be derived from cellular toxicity of large amount of liposome. Li et al. reported that cell viability decreased along with the increase in microbubble concentration [1]. Guo et al. demonstrated that cell viability decreased with the increase in duration of insonification [7]. Suzuki et al. and Li et al. showed that cell viability decreased with the increase in ultrasound acoustic pressure [8, 9].

On the basis of those previous findings, we planned to examine the effects of amount of plasmid DNA, liposome concentration, duration of insonification, repeat count of insonification, and time of incubation with liposome, cell, and DNA on transfection rate, which was measured by means of HGF protein release into culture medium.

2. Materials and Methods

2.1. Cell Culture. Primary cultures of neonatal ventricular myocytes were prepared as described previously [10]. Briefly, apical halves of cardiac ventricles from 1-day-old Wistar rats were separated, minced, and dispersed with 0.1% collagenase type II (Worthington Biochemical Corp., Freehold, NJ). Myocytes were segregated from nonmyocytes using a discontinuous Percoll gradient (Sigma Chemical Co., Inc., St. Louis, MO). After centrifugation, the upper layer consisted of a mixed population of nonmyocyte cell types and the lower layer consisted almost exclusively of cardiac myocytes. After the myocytes had been incubated twice on uncoated 10-cm culture dishes for 30 minutes to remove any remaining nonmyocytes, the nonattached viable cells were plated on gelatin-coated 24-well culture plates or 10-cm culture dishes and then cultured in DMEM (Life Technologies, Grand Island, NY) supplemented with 10% FCS (Life Technologies, Grand Island, NY). After 24-hour incubation in DMEM with FCS, the culture medium was changed to serum-free DMEM, and all experiments were performed 24 hours later. This purification procedure has well been established [11, 12], and >95% of the cells obtained by this method were cardiomyocytes.

2.2. Plasmid DNA. Preparation of rat hepatocyte growth factor (HGF) expression plasmid DNA was described previously [13]. Briefly, rat HGF cDNA cloned by polymerase chain reaction was inserted into the unique Xho I site between the cytomegalovirus immediate-early enhancer-chicken β-actin hybrid promoter and rabbit β-globin poly A site of the pCAGGS expression plasmid [14]. The resulting plasmid, pCAGGS-HGF, was grown in Escherichia coli DH5α (Figure 1(a)). The plasmid was purified with a QUIAGEN plasmid DNA kit and dissolved in TE buffer. The purified plasmid DNA was stored at -20°C and diluted to the required concentration with distilled water immediately before use.

2.3. Bubble Liposome. Liposome microbubble, SHU 508A, consists of palmitic acid and galactose and provides echogenic micron-sized air bubbles when suspended in water. The diameter of bubbles ranges from 2 to 8 μm, and 97% are smaller than 6 μm [15]. These air bubbles are stabilized by palmitic acid, which forms a molecular film that lowers the surface tension of the aqueous vehicle. The SHU 508A bubbles are nontoxic, have a neutral pH, are biodegradable, and are made from a physiologically occurring substance. The physiochemical properties of SHU 508A bubbles are typical of a saccharide solution [15].

2.4. Experiment on Ultrasound Mode. Before performing the experiments for dose-effect relationships using liposome sonoporation, we needed to determine the most appropriate ultrasound mode for the sonoporation procedure for efficient transfection. We tested four modes of ultrasound: pulsed wave Doppler, color flow Doppler, continuous wave Doppler, and harmonic power Doppler, which are available with standard echocardiographic machinery in a clinical laboratory. We performed a simple transfection experiment at the same acoustic pressure of 0.5 W/cm^2 for each ultrasound mode, using a single condition with 60 μg HGF plasmid DNA, 1×10^7 particles/mL of SHU 508A liposome, 30 sec insonification, 15 min of DNA incubation, and 3 repetitions of insonification.

Rat neonatal cardiomyocytes were inoculated and grown to confluence in DMEM+10% FCS. After confluence had been reached in a 35 mm Petri dish, the medium was changed to fresh defined serum-free medium. Plasmid DNA was diluted with distilled water immediately before the transfection. Each experiment was performed on 20 dishes. Cells on each dish were treated with ultrasound (Figure 1(b)). Pulsed wave Doppler, color flow Doppler, and continuous wave Doppler were insonified from PSK-25AT acoustic transducer with Toshiba SSA-380A (Toshiba Medical Systems), and harmonic power Doppler was insonified from S3 transducer with Sonos 5500 (Phillips Medical Systems). The experimental results are shown in Figure 2. Continuous-wave Doppler ultrasound was the most efficacious and was used for subsequent experiments.

2.5. Experiments for Dose-Effect Relations. The medium in 35 mm Petri dishes containing the cardiomyocytes was changed to fresh defined serum-free medium from DMEM+10% FCS. Rat HGF plasmid DNA was diluted with distilled water, and a volume corresponding to 60, 120, or 180 μg was added to each of the 20 Petri dishes per DNA dose. Cells on each dish were then treated with continuous-wave Doppler ultrasound (frequency of 2.5 MHz and acoustic intensity of 0.5 W/cm^2 from a PSK-25AT acoustic transducer with Toshiba SSA-380A Ultrasound system) with SHU 508A liposome (1×10^7 particles/mL) for acoustic exposure time of 30 or 60 seconds at room temperature (Figure 1(b)). In a separate series of experiments, we tested four liposome

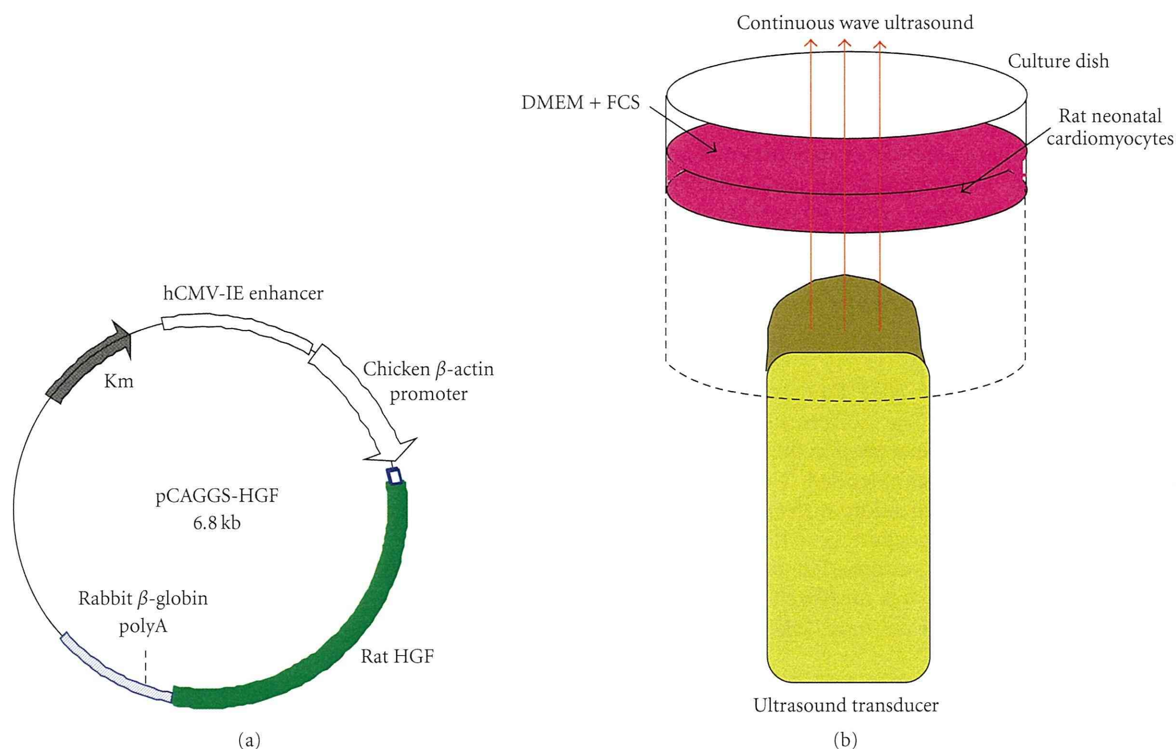

Figure 1: (a) Structure of the expression plasmid pCAGGS-HGF. The expression cassette of pCAGGS-HGF contains chicken β-actin promoter, rat HGF, and rabbit β-globin poly A. (b) Experimental setup. The transducer was attached to the bottom of the dish.

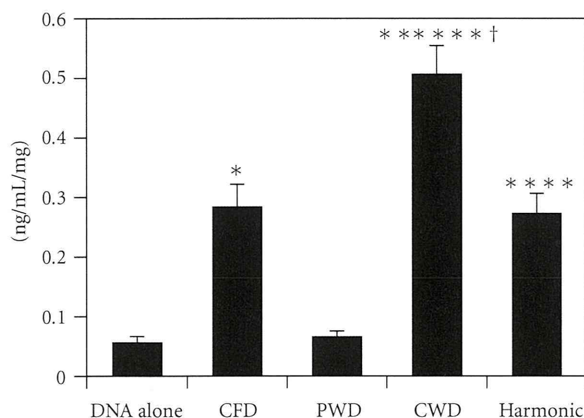

Figure 2: Comparison of four modes of ultrasound for sonoporation. Cells treated with continuous-wave Doppler ultrasound yielded the largest amount of HGF protein indicating this to be the most effective ultrasound mode. CFD: color flow Doppler; PWD: pulsed wave Doppler; CWD: continuous wave Doppler; Harmonic: harmonic power Doppler. $^{*}P < .05$ versus DNA alone; $^{**}P < .05$ versus CFD; $^{***}P < .05$ versus PWD; $^{\dagger}P < .05$ versus Harmonic.

concentrations (0, 1×10^6, 1×10^7 or 1×10^8 particles/mL), three insonification repetitions (1 insonification only, 3 or 5 insonifications for 30 seconds), and three DNA incubation times (15, 60 or 120 min). After the incubation, the culture medium was changed to normal DMEM+10% FCS and the cells were cultured for 72 hours. In a separate set of experiments, we examined the effect of culture period on the amount of DNA product that is HGF protein by discontinuing culture at 24, 48, and 72 hours and measuring the amount of rat HGF protein in the medium. The total amount of protein content in the cultured cells was measured and used to correct the HGF level in each dish. We measured rat HGF protein using an EIA kit (Institute of Immunology Co., Ltd., Tokyo, Japan) [13] and protein content of cultured cells using a Modified Lowry Protein Assay Kit (Pierce Biotechnology, Rockford).

2.6. Viability of Cultured Cells. To determine the safety of sonoporation, in a separate experiment, cultured cells were exposed to 0.1% trypan blue for 5 min just after ultrasound insonification. This allowed assessment of sarcolemmal membrane damage and was performed for each concentration of liposome, each insonification time, and each number of repetitions of insonification. The number of stained and unstained cells in the dishes was counted and used to calculate the percentage of intact cells [16]. The degree of cellular injury caused by sonoporation was determined by examining the insonified cells by scanning electron microscopy (Hitachi S-4800). Immediately after ultrasound insonification in the presence of liposome, the cardiomyocytes were fixed with phosphate-buffered 2.5% glutaraldehyde for 4 hours, followed by postfixation with 1%

osmium tetroxide for 1 hour, and then were conventionally prepared for scanning electron microscopy.

2.7. Statistical Analysis. Data were expressed as the mean ± SEM. Comparisons of parameters from experimental groups were performed with unpaired t tests and resulting P-values were corrected according to the Bonferroni method. In analyses, $P < .05$ was considered to indicate statistical significance.

3. Results

3.1. Effect of Culture Period on HGF Protein Production by Sonoporated Cardiomyocytes. The concentration of HGF protein in the culture medium increased as the culture period after ultrasonic transfection was extended. The transfection consisted of three 30-sec insonifications a 15-min incubation with HGF DNA (60 μg) and liposome (1×10^7 particle/mL) (Figure 3(a)). After 72 hours of culture, HGF protein concentration in the culture medium was measured and corrected using the protein content of the cultured cells.

3.2. Effect of the Amount of Plasmid DNA on HGF Protein Production by Sonoporated Cardiomyocytes. HGF protein concentration in the culture medium was 0.54 ± 0.049 ng/mL/mg and was highest when 60 μg of DNA was administered with a liposome concentration of 1×10^7 particles/mL, a15-min incubation, and three 30-sec insonification. Although the nominal mean values of HGF protein after transfection of 120 and 180 μg DNA were lower than those after transfection of 60 μg, the differences were not statistically significant (Figure 3(b)).

3.3. Effect of Incubation Period with Plasmid DNA and Liposome on HGF Protein Production by Sonoporated Cardiomyocytes. HGF protein concentration in the culture medium was 0.56 ± 0.053 ng/mL/mg and was highest when the incubation time was 15 min with a liposome concentration of 1×10^7 particles/mL, 60 μg DNA, and three 30-sec insonification. Although the mean values of HGF protein after transfection for 60 and 120 min were lower than those after 15 min incubation, the differences were not statistically significant (Figure 3(c)).

3.4. Effect of Insonification Time on HGF Protein Production by Sonoporated Cardiomyocytes. HGF protein concentration in the culture medium was 0.59 ± 0.052 ng/mL/mg and was highest when the insonification period was 30 sec with 60 μg DNA, a liposome concentration of 1×10^7 particles/mL, and 15-min incubation. There was no significant difference in HGF production in cells insonified for 30 and 60 min (Figure 3(d)).

3.5. Effect of Liposome Concentration on HGF Protein Production by Sonoporated Cardiomyocytes. HGF protein concentration in the culture medium was 0.53 ± 0.053 ng/mL/mg and was nominally highest when the liposome concentration was 1×10^7 particles/mL and insonification consisted of three 30-sec ultrasound exposures, though it was statistically similar to that obtained with 1×10^6 particles/mL. At a higher liposome concentration of 1×10^8 particles/mL, HGF protein concentration decreased (Figure 3(e)).

3.6. Effect of Repetition of Insonification on HGF Protein Production by Sonoporated Cardiomyocytes. HGF protein concentration in the culture medium was 0.54 ± 0.053 ng/mL/mg and was highest when three 30-sec insonifications were given, with a liposome concentration of 1×10^7 particles/mL and 60 mg DNA. This protein production was statistically higher than in cells given one or five insonifications (Figure 3(f)).

3.7. Effect of Insonification Time on Cell Viability. The percentage of dead cells was 14.7 ± 0.9% and was higher in the cells given five 30-sec insonifications at a liposome concentration of 1×10^7 particles/mL (Figure 4(a)). There was no statistical difference between 30- and 60-sec insonification.

3.8. Effect of Liposome Concentration on Cell Viability. The percentage of dead cells increased with increasing concentrations of liposome (Figure 4(b)). The dead cell count was 24.8 ± 2.9% and was highest when the liposome concentration was 1×10^8 particles/mL and three 30-sec insonifications were used.

3.9. Effect of Number of Insonification Repetitions on Cell Viability. The percentage of dead cells increased as the number of insonification repetitions increased (Figure 4(c)). The dead cell count was 14.7 ± 0.9% and was highest when five repetitions of the insonification step were given, with a liposome concentration of 1×10^7 particles/mL.

3.10. Scanning Electron Microscopy Observations of Sonoporated Cardiomyocytes. No particular changes were evident on the surfaces of untreated control cultured cardiomyocytes when viewed with the scanning electron microscope at low and high magnification (Figures 5(a) and 5(b)). After sonoporation with a low concentration of liposome (Figure 5(c)) and with a high concentration of liposome (Figure 5(d)), microdimples or pores were observed on the surfaces of the cultured cardiomyocytes.

4. Discussion

Considerable efforts have been made to develop methods that will allow effective and safe introduction of vectors into cells for gene therapy. However, we still need a breakthrough in the form of a novel vector that will transform cells at high efficiency and with low risk of adverse effects. This is especially true in cardiovascular medicine, where malignant cellular transformation is rare [17]. One of the promising candidates for safe and efficacious gene transfection is a naked plasmid vector that has been modified to have high affinity for cardiovascular tissues but which has no built-in viral components [17, 18]. We have developed a method for electroporation of a cytokine gene for treatment of

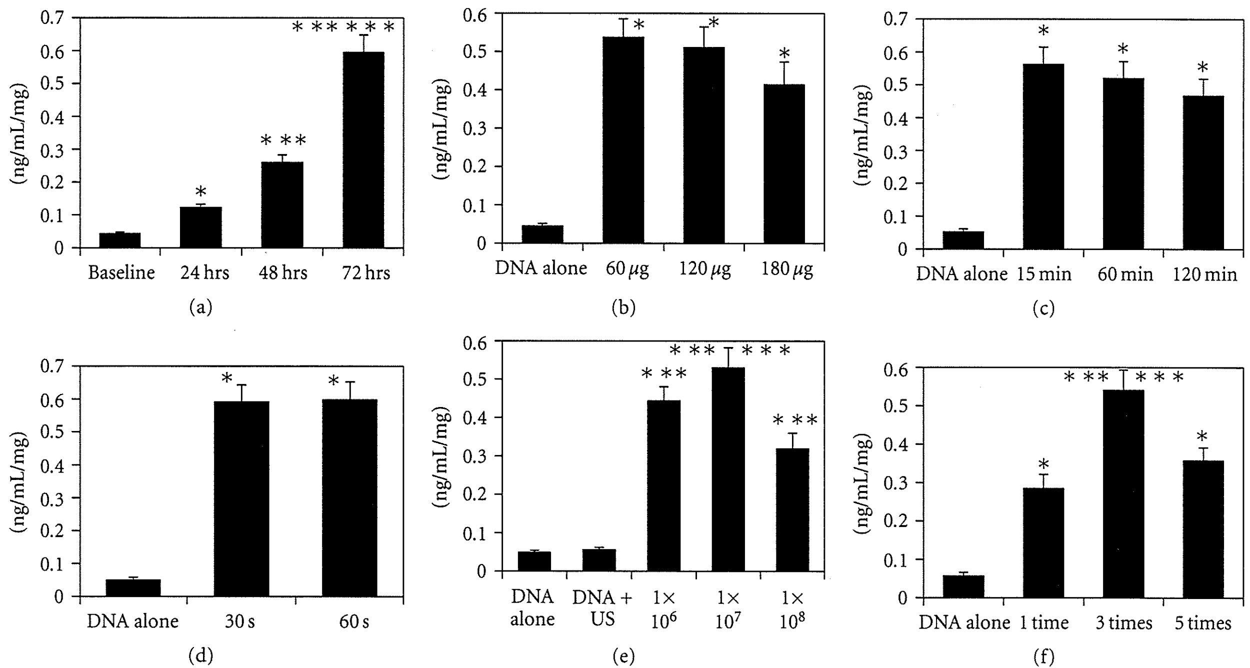

Figure 3: (a) Effect of culture period after transfection of HGF DNA on HGF protein production using 60 μg of DNA and 1×10^7 particles/mL liposome with three 30-sec insonifications and 15-min incubation with DNA. Baseline was the concentration of rat HGF protein in the culture medium around rat cardiomyocytes without any intervention at the beginning of cell culture. $*P < .05$ versus baseline; $**P < .05$ versus 24 hours after the onset of culture; $***P < .05$ versus 48 hours after the onset of culture. (b) Effect of amount of plasmid DNA on HGF protein production using 1×10^7 particles/mL liposome with three 30-sec insonifications and 15-min incubation with DNA. "DNA alone" indicates the concentration of rat HGF protein in the culture medium of cardiomyocytes treated with 60 μg DNA without insonification. $*P < .05$ versus DNA alone. (c) Effect of incubation period of cardiomyocytes with plasmid DNA and liposome on HGF protein production using 60 μg of DNA and 1×10^7 particles/mL liposome with three 30-sec insonifications. $*P < .05$ versus DNA alone. (d) Effect of insonification time on protein production using 60 μg of DNA, 1×10^7 particles/mL liposome, and 15-min incubation with DNA, and three 30- or 60-sec insonifications. $*P < .05$ versus DNA alone. (e) Effect of liposome concentration on HGF protein production using 60 μg of DNA with three 30-sec insonifications and 15-min incubation with DNA. $*P < .05$ versus DNA alone; $**P < .05$ versus 0 particles/mL; $***P < .05$ versus 1×10^8 particles/mL. (f) Effect of repetition of insonification on HGF protein production using 6 μg of DNA and 1×10^7 particles/mL liposome with 15-min incubation with DNA. $*P < .05$ versus DNA alone; $**P < .05$ versus 1 time; $***P < .05$ versus 5 times.

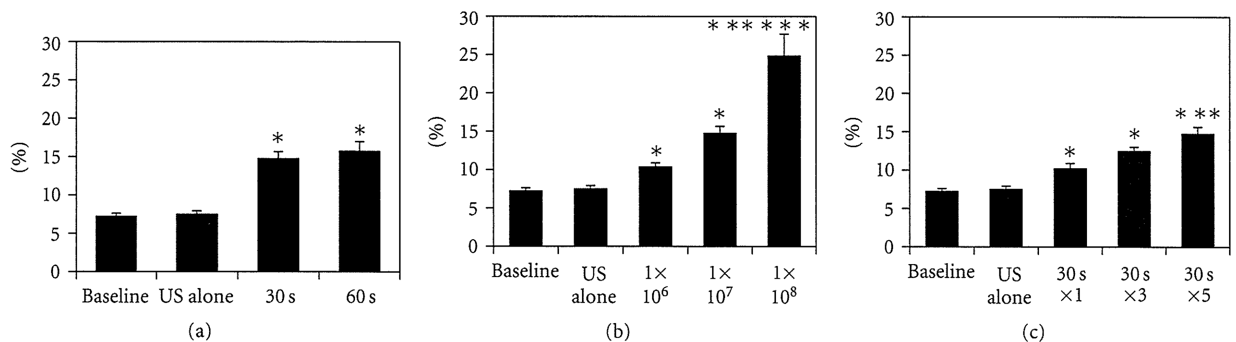

Figure 4: (a) Effect of insonification time on cell viability using 60 μg of DNA, 1×10^7 particles/mL liposome, and 15-min incubation with DNA, and three 30- or 60-sec insonifications. "US alone" represents the percentage of dead cells immediately after three 30-sec insonifications in the absence of liposome and DNA. $*P < .05$ versus baseline. (b) Effect of liposome concentration on cell viability using 60 μg of DNA and three 30-sec insonifications and 15-min incubation with DNA. $*P < .05$ versus baseline; $**P < .05$ versus 1×10^6 particles/mL; $***P < .05$ versus 1×10^8 particles/mL. (c) Effect of repetitions of insonification on cell viability using 60 μg of DNA, 1×10^7 particles/mL liposome, and 15-min incubation with DNA. $*P < .05$ versus baseline; $**P < .05$ versus 30 sec $\times$ 1.

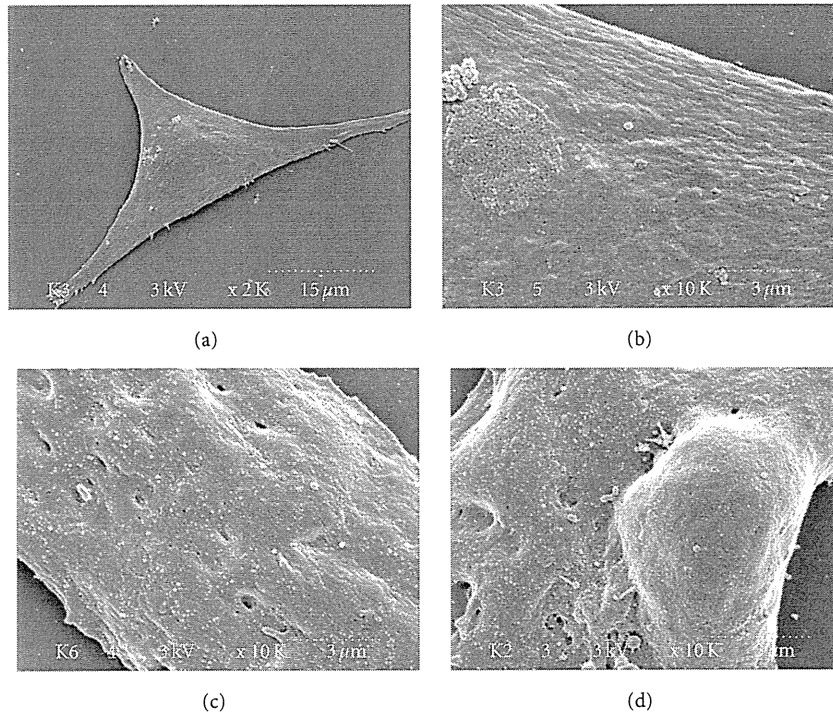

(a) (b) (c) (d)

FIGURE 5: (a) and (b) Scanning electron microscopic images of intact cell surfaces of cultured cardiomyocytes. Scale dots are indicated on the images. (c) Image of a cell surface immediately after sonoporation using 1×10^6 particles/mL liposome. (d) Image of a cell surface immediately after sonoporation using 1×10^8 particles/mL liposome.

cardiomyopathy [13]. However, using electric shock for transfection is not clinically practical. For this reason, we are pursuing the present sonoporation method as a protocol for gene transfection.

The HGF protein used in the present study is found in a wide variety of cell types and has multiple biological properties, including mitogenic, motogenic, morphogenic and antiapoptotic activities [19]. Several lines of evidence indicate that this molecule has potential for therapeutic use for treatment of heart failure, myocardial infarction, angina, and hypertension [20–22]. HGF may also have enormous therapeutic potential for hepatic and renal disorders, in addition to cardiovascular diseases [23–26].

In the present study, we showed variations in amount of HGF plasmid DNA, liposome concentration, the duration of insonification, and incubation time of the cardiomyocytes with liposome and DNA, and their dose relationships with the final amount of HGF protein released from the cultured neonatal cardiomyocytes. We found that specific amounts of liposome and repetitions of insonification were needed for effective protein production from cardiomyocytes. However, high concentrations of bubble liposome and large numbers of repeat insonifications resulted in decreased cell viability.

Plasma membrane sonoporation induced by ultrasound and subsequent self-sealing has been reported in previous investigations [27–29]. However, the exact mechanism by which membrane sonoporation causes substance incorporation into the cell is not yet understood. Some investigators speculate that the membrane poration results in both transfection efficiency and cellular damage. In the present study, scanning microscopy images revealed some microdimples or pores on the cell surface after sonoporation, which did not exist on the surface of control cardiomyocytes. The numbers of dimples or pores tended to increase with higher concentrations of liposome. Thus, we speculate that these dimples or pores on the cell surface might be related to transfection efficiency and might be evidence of cellular injury by sonoporation. Previous studies of sonoporation of vascular walls revealed that microbubble destruction would cause rupture of microvessels and extravasation [30–33], which would cancel out some benefits of sonoporation. Thus, the poration and self-sealing mechanism needs to be fully investigated and optimized.

A sonoporation technique targeting the cardiovascular system has now been developed for gene transfection to myocardium, limb skeletal muscle, and arteries [34–37]. For a variety of target tissues, a number of microbubbles, including liposomes, and a range of ultrasound modes have been developed. The optimal combination of the type of microbubble, ultrasound mode, and target tissue still needs to be resolved [38–40]. However, the principal types of ultrasound used for sonoporation have included pulsed wave Doppler or continuous wave Doppler with acoustic pressure ranging 0.5–5 W/cm^2 [34–37]. In the present study, we found that continuous wave Doppler at a standard frequency for clinical use, that is, 2.5 MHz and the usual acoustic pressure of 0.5 W/cm^2, was most effective with our cardiomyocytes.